Selective eradication of cancer displaying hyperactive Akt by exploiting the metabolic consequences of Akt activation

Veronique Nogueira[1*], Krushna C. Patra[1,3], and Nissim Hay[1,2*]

[1]Department of Biochemistry and Molecular Genetics, College of Medicine, University of Illinois at Chicago, Chicago, IL 60607, USA [2]Research & Development Section, Jesse Brown VA Medical Center, Chicago, IL 60612, USA

[3] Present address: Massachusetts General Hospital Cancer Center, Harvard Medical School, Boston, MA 02114, USA

- Correspondence: Nissim Hay (nhay@uic.edu), Veronique Nogueira (vnogueir@uic.edu) Tel: 312-355-1684

Department of Biochemistry and Molecular Genetics, College of Medicine, University of Illinois at Chicago, Chicago, IL 60607, USA

Conflict of Interest: There is no conflict of interest to declare

Abstract

Akt activation in human cancers exerts chemoresistance, but pan-Akt inhibition elicits adverse consequences. We exploited the consequences of Akt-mediated mitochondrial and glucose metabolism to selectively eradicate and evade chemoresistance of prostate cancer displaying hyperactive Akt. PTEN-deficient prostate cancer cells that display hyperactivated Akt have high intracellular reactive oxygen species (ROS) levels, which are due, in part, to Akt-dependent increase of oxidative phosphorylation. High intracellular ROS levels selectively sensitize cells displaying hyperactive Akt to ROS-induced cell death enabling a therapeutic strategy combining a ROS inducer and rapamycin in PTEN-deficient prostate tumors in mouse models. This strategy elicited tumor regression, and markedly increased survival even after the treatment was stopped. By contrast, exposure to antioxidant increased prostate tumor progression. To increase glucose metabolism Akt activation phosphorylates HK2 and induced its expression. Indeed, HK2 deficiency in mouse models of Pten-deficient prostate cancer elicited a marked inhibition of tumor development and extended lifespan.

Introduction

One of the most frequent events in human cancer is hyperactivation of the serine/threonine kinase Akt. Akt is hyperactivated in cancer by multiple mechanisms, largely through the activation of its upstream regulator phosphoinositide 3-kinase (PI3K), which generates the phosphatidylinositol-3,4,5-trisphophate (PIP_3) required for Akt activation (Mayer & Arteaga, 2016). The activity of PI3K is negatively regulated by the tumor suppressor Phosphatase And Tensin Homolog (PTEN), which is a PIP3 phosphatase, and therefore inhibits the PI3K/Akt signaling pathway. PTEN expression is frequently lost in human cancers, specifically in glioblastoma, melanoma, endometrial and prostate cancers (Hollander, Blumenthal et al., 2011). The frequent activation of PI3K/Akt signaling in cancer and its ability to exert chemoresistance led to the development of small molecule inhibitors of PI3K and Akt, which are currently being tested in clinical trials (Kim, Dan et al., 2005, Zhang, Kwok-Shing Ng et al., 2017, Zheng, 2017). There are three Akt genes in mammalian cells (*Akt1-3*), and their encoded proteins have a high degree of identical amino acids. The expression pattern in mammalian tissues and organs is different amongst the three isoforms. While Akt1 is ubiquitously expressed, Akt2 is expressed at the highest level in insulin-responsive tissues, and Akt3 is expressed at the highest level in the brain. The different mouse phenotypes with the individual Akt isoform germ line deletions can be explained by their relative expression in the organs that determine the phenotype (Dummler & Hemmings, 2007, Hay, 2011). The Akt inhibitors currently in clinical trials are pan-Akt inhibitors that inhibit the different Akt isoforms to a similar extent. These pan-Akt inhibitors exert undesired side effects, such as hyperglycemia, hyperinsulinemia, and diabetes (Wang, Chen et al., 2017). Furthermore, genetic deletion of Akt1 and Akt2 in the mouse liver induces liver damage, inflammation, and paradoxically hepatocellular carcinoma (HCC) (Wang, Yu et al., 2016). Therefore, developing isoform-specific inhibitors could reduce the undesired systemic consequences of pan-Akt inhibition, although this is challenging. Alternatively, a therapeutic approach that selectively targets cancer cells displaying hyperactive Akt should be developed.

Perhaps the most evolutionarily conserved function of Akt is mediating cellular and organismal metabolism. This conserved function of Akt is likely utilized by cancer cells to fulfill their anabolic demands. Since PTEN is lost in approximately 40% of prostate cancers

(Pourmand, Ziaee et al., 2007, Taylor, Schultz et al., 2010), we chose to work towards developing a personalized therapeutic approach by using PTEN-deficient prostate cancer to explore selective vulnerability as a consequence of Akt's metabolic activity. As we showed previously, activation of Akt increases both glycolysis and oxidative phosphorylation (Gottlob, Majewski et al., 2001, Robey & Hay, 2009). We also showed that Akt activation increases intracellular ROS levels, in part by increasing oxidative phosphorylation. Since Akt does not exert resistance to ROS-induced cell death, increasing ROS levels could selectively eradicate cells displaying hyperactive Akt (Nogueira, Park et al., 2008). Here, we showed that human PTEN-deficient and not PTEN-proficient prostate cancer cells have high intracellular ROS levels, which are Akt-dependent. The high level of ROS can be exploited to selectively eradicate human PTEN-deficient tumors in vivo as well as in a mouse model of Pten-deficient prostate cancer. We used the natural compound phenylethyl isothiocyanate (PEITC) that depletes intracellular glutathione (Xu & Thornalley, 2001) as a ROS inducer either alone or in combination with the mTORC1 inhibitor rapamycin to selectively eradicate Pten-deficient cancer cells in vivo. We also found that in PTEN-deficient prostate cancer, HK2 is induced because of Akt activation to increase glycolysis. HK2 is the hexokinase isoform that is not highly expressed in most mammalian tissues but is generally induced in cancer cells by multiple mechanisms (Hay, 2016). Furthermore, HK2 is phosphorylated by Akt to increase its mitochondrial binding (Miyamoto, Murphy et al., 2008) and therefore its glycolytic activity (DeWaal, Nogueira et al., 2018). Here we showed that silencing HK2 in human PTEN-deficient prostate tumors and deleting HK2 in a mouse model of Pten-deficient prostate cancer inhibits cancer development in both cytostatic and cytotoxic manners. HK2 deficiency also overcame the chemoresistance of PTEN-deficient prostate cancer cells.

Results

PTEN-deficient human prostate cancer cells display high oxygen consumption, OXPHO and high levels of ROS

We employed three human prostate cancer cell lines: DU145, which is PTEN-proficient, and PC3 and LNCaP, which are PTEN-deficient. As expected, the PTEN status in DU145, PC3 and LNCaP cells determines Akt activity in these cells (Figure 1A). DU145 cells, which harbor wild-type PTEN, exhibit low Akt activity. PTEN-deficient PC3 and LNCaP cells display

hyperactivated Akt. As we previously found, Akt elevates oxygen consumption and intracellular ROS levels (Nogueira et al., 2008). We therefore determined these two parameters in prostate cancer (CaP) cells in which PTEN is frequently lost. Basal oxygen consumption was the lowest in the PTEN-proficient DU145 cells, while it was gradually increased in the PTEN-deficient PC3 and LNCaP cells (Figure 1B), following the pattern of Akt activity in which higher oxygen consumption was correlated with higher Akt activity. Silencing Akt1 and Akt2 in PC3 cells markedly decreased oxygen consumption, indicating that the high oxygen consumption in these cells is Akt-dependent (Figure 1C). Interestingly, basal oxygen consumption in DU145 cells reached the maximum capacity of the respiratory chain, while PC3 and LNCaP cells have a larger spare capacity. Fig. 1B also shows that the ATP production capacity is two-fold higher in PC3 and LNCaP cells compared to DU145 cells, agreeing with our previous observations that Akt activation increases ATP production by both glycolysis and oxidative phosphorylation (Gottlob et al., 2001). Since intracellular ROS are by-products of high OXPHO, we determined intracellular ROS production at the cytosolic (Figure 1D) and mitochondrial (Figure 1E) levels, and found that high Akt activity was correlated with high intracellular levels of ROS. Akt1 and Akt2 knockdown in PC3 cells consistently decreased ROS levels, confirming that Akt regulates intracellular ROS levels. (Figure 1F). Finally, we found that in PC3 and LNCaP cells mitochondrial membrane potential is higher than in DU145 cells (Figure 1-figure supplement 1), which is likely correlated with the higher respiratory chain activity in PC3 and LNCaP cells.

In our previous studies, we found that Akt activation increases ROS not only by increasing oxygen consumption but also by inhibiting the expression of ROS scavengers downstream of FOXO, such as MnSOD and catalase, and particularly sestrin3 (Sesn3) (Nogueira et al., 2008). Sesn3 is a transcriptional target of FOXO (Chen, Jeon et al., 2010) and a member of a protein family including Sesn1 and Sesn2, which reduce ROS by several mechanisms (Bae, Sung et al., 2013, Kopnin, Agapova et al., 2007). Interestingly, in contrast to our findings in MEFs (Nogueira et al., 2008), changes in MnSOD and catalase expression in the CaP cells did not correlate with changes in ROS levels (Figure 1-figure supplement 2), which is consistent with what was previously observed (Chowdhury, Raha et al., 2007). However, the pattern of Sesn3 expression was consistent with ROS levels, and while DU145 cells express high levels of Sesn3, PC3 and LNCaP cells express relatively low levels of Sesn3 (Figure 1-figure supplement 3). Interestingly, downregulation of Sesn3 in DU145 cells or up-regulation of Sesn3 in PC3 cells (Figure 1-figure

supplement 4) was sufficient to modulate cytosolic ROS production in these cells (Figure 1-figure supplement 5Sesn3 knockdown in DU145 cells increased ROS production, while overexpression of Sesn3 in PC3 cells decreased ROS production. These results suggest that Sesn3 contributes to the regulation of intracellular ROS downstream of Akt and FoxOs in CaP cells.

Taken together, these results show that PTEN-deficient prostate cancer cells display high OXPHO and ROS levels in an Akt-dependent manner.

PTEN-deficient prostate cancer cells are selectively sensitized to killing by a ROS inducer

We previously reported that cells that display high Akt activity could be selectivity killed by increasing the intracellular level of ROS (Nogueira et al., 2008). This selectivity is due to the high intracellular ROS levels exerted by Akt activation in combination with the inability of Akt to protect against ROS-induced cell death. We therefore treated the prostate cancer cells with 2-methoxyestradiol (2-ME), an endogenous metabolite of estradiol-17beta that increases ROS, or with β-phenylethyl isothiocyanate (PEITC), a natural compound found in consumable cruciferous vegetables that is known to increase intracellular ROS levels by depleting intracellular glutathione (Ting, Lee et al., 2010) (Yu, Mandlekar et al., 1998) (See also Figure 2-figure supplement 1 We found that CaP cells with high Akt activity due to the loss of PTEN (LNCaP, PC3 cells) were more vulnerable to 2-ME- and PEITC-induced cell death than the PTEN-proficient CaP cells (DU145 cells) (Figure 2 A, B, and Figure 2-figure supplement 2). Consistently LNCaP and PC3 cells are more vulnerable to the glutathione reducing agent BSO (Figure 2-figure supplement 3). Interestingly, NADP+/NADPH ratio is elevated in the PTEN-deficient cells (Figure 2-figure supplement 4). The elevated NADP+/NADPH could be either contributing to the high level of ROS or it is a result of increased NADPH consumption to combat the high ROS level. Alternatively or additionally, higher NADPH is consumed for fatty acid synthesis in the PTEN-deficient cells can contribute to the higher NADP+/NADPH ratio.

Silencing Sesn3 increased PEITC-induced cell death in DU145 cells, and overexpression of Sesn3 in PC3 cells decreased their sensitivity to PEITC (Figure 2-figure supplement 5). The cell death induced by PEITC is ROS-dependent since it is inhibited by the ROS scavenger N-acetyl cysteine (NAC) (Figure 2-figure supplement 6). To determine if the hypersensitivity of PTEN-deficient prostate cancer cells to ROS-induced cell death is PI3K/Akt dependent, we first restored

PTEN expression in the Pten-deficient cells and silenced Pten in the Pten-proficient cells. (Figure 2-figure supplement 7). Oxygen consumption and ROS production were increased by silencing PTEN in DU145 cells and decreased in PC3 and LNCaP cells expressing PTEN (Figure 2-figure supplement 8). The silencing of PTEN in DU145 cells increased sensitivity to PEITC, whereas the expression of PTEN in PC3 and LNCaP cells decreased their sensitivity to PEITC (Figure 2-figure supplement 9). Like the silencing of PTEN in DU145 cells expression of activated myristoylated Akt (mAkt) in DU145 cells increased ROS levels and renders the cells more sensitive to ROS-induced cell death (Figure 2-figure supplement 10). Finally, the knockdown of Akt1 and Akt2 in PC3 and LNCaP cells that reduced ROS levels also rendered them resistant to PEITC-induced cell death (Figure 1F, Figure 2C, and Figure 2-figure supplement 11). We concluded that Akt activation in Pten-deficient prostate cancer cells could not protect against oxidative stress-induced cell death but rather sensitized the cells to ROS-induced cell death by increasing their intracellular ROS levels.

Treatment with PEITC and rapamycin inhibits and regresses tumor development in a xenograft model and in a mouse model of prostate cancer

We previously showed that rapamycin treatment could further sensitize cells displaying hyperactive Akt to oxidative stress-induced cell death, which could be due, in part, to the further activation of Akt by the inhibition of mTORC1 inhibitory activity on the PI3K/Akt signaling (Nogueira et al., 2008). This was also observed in prostate cancer cells (Figure 2-figure supplement 12). Thus, the combination of rapamycin and oxidative stress could not only circumvent resistance to cell death but also selectively kill cells treated with rapamycin. Before applying this strategy to animal models of prostate cancer, we first established our proof-of-concept with prostate cancer cells in vitro. As shown in Figure 2D, rapamycin alone did not induce cell death, but pretreatment with rapamycin augmented the ability of PEITC to induce cell death in all 3 CaP cell lines. Although rapamycin treatment increased PEITC-induced cell death in all cell lines, the LNCaP and PC3 cells with hyperactivated Akt were markedly more sensitive to cell death induced by the combination of rapamycin and PEITC than DU145 cells (Figure 2D). The synergistic effect of rapamycin and PEITC on cell death could be explained by the induction of ROS exceeding the scavenging capacity (Figure 2-figure supplement 13). We found that rapamycin, by itself, does not substantially affect oxygen consumption or intracellular

ROS induced by Akt (Figure 2-figure supplement 14). This contrasts with the catalytic inhibitor of mTOR, torin1, which decreased oxygen consumption and ROS levels (Figure 2-figure supplement 14). These results are consistent with previously published results showing that while the mTOR kinase inhibitor inhibits OXPHO in an eIF4E-dependent manner, rapamycin does not (Morita, Gravel et al., 2013). We concluded that combining rapamycin and PEITC could be used to selectively kill prostate cancer cells expressing hyperactive Akt.

To examine the efficacy of the strategy to selectively eradicate prostate cancer cells carrying activated Akt in vivo, we first employed xenografts of PC3 cells in athymic nude mice and studied the effect of PEITC and rapamycin on the growth of tumors induced by PC3 cells (Figure 2E). After tumor onset, the mice were either not treated or treated with either rapamycin alone, PEITC alone or the combination of both rapamycin and PEITC. Rapamycin alone or PEITC alone significantly attenuated the growth of the tumors, but the tumors remained palpable. However, the combination of PEITC and rapamycin regressed tumor growth and eradicated the tumors. Analyses of tumor sections near the endpoint of the experiment showed that PEITC alone induced both a profound inhibition of BrdU incorporation and cell death, as assessed by cleaved caspase 3, whereas rapamycin alone did not induce cell death but did inhibit BrdU incorporation (Figure 2F-H). Cell death after treatment with both PEITC and rapamycin, as measured by cleaved caspase 3, was profoundly higher than that induced by PEITC alone (Figure 2F-H). When the PTEN-proficient DU145 xenografts were similarly treated, the effect of rapamycin alone or PEITC alone on tumor growth was not as profound (Figure 2-figure supplement 15). Importantly, the combination of rapamycin and PEITC did not decrease tumor growth as it did for the PTEN-deficient PC3 xenografts. Thus, these results indicate that the combination of rapamycin and PEITC could be an effective therapeutic strategy for PTEN-deficient prostate cancer or prostate cancer in which Akt is hyperactivated.

To further address the feasibility of PEITC and rapamycin treatment for PTEN-deficient prostate cancer, we employed a mouse model for prostate cancer in which prostate Pten is specifically deleted by Cre recombinase driven by the probasin promoter (*Pbsn-Cre4;Pten*$^{f/f}$ mice). Mice that are deficient for PTEN in the prostate display progressive forms of prostatic cancer that histologically resemble human prostate cancer, ranging from mild prostatic intraepithelial neoplasia (PIN) at 10 weeks of age to large multinodular malignant adenocarcinoma with metastasis within 8 months (Trotman, Niki et al., 2003). Pten deletion

leads to Akt activation in the prostate and, similar to what we observed in vitro, an increase in oxidative stress, as measured by the increased level of 4-hydroxynonenal (4HNE) protein adducts (Figure 3A). Since the onset of PIN occurs within 2 months and invasive CaP occurs within 8 months, we could test the efficacy of our therapeutic approach at two different stages of prostate cancer, low-grade PINs and, later, high-grade PINs and CaP stages. The first strategy is depicted in Figure 3B. The treatment did not significantly affect the mice body weights (Figure 3-figure supplement 1), and the prostate weights did not significantly change in the control mice after treatment with rapamycin alone, PEITC alone or rapamycin and PEITC in combination (Figure 3-figure supplement 2). However, these treatments significantly decreased the prostate weights in the *Pbsn-Cre4;Pten*$^{f/f}$ mice, which was most profound when both rapamycin and PEITC were combined (Figure 3C). When tumor sections were analyzed after 8 months, we found that all treatments markedly inhibited proliferation, as measured by BrdU incorporation (Figures 3D and 3E), but PEITC also induced cell death, which was further exacerbated when PEITC was combined with rapamycin (Figures. 3D and 3F). Finally, the combination of rapamycin and PEITC treatment markedly increased survival (Figure 3G). Histopathological analysis showed that while two third and one third of untreated mice had high grade PIN and microinvasive carcinoma respectively, one third of mice treated with rapamycin and PEITC did not have any detectable PIN, 16% had low grade PIN and only one third had high grade PIN and 16% microinvasive carcinoma (Table 1, and Figure 3-figure supplement 3). By contrast, treating the mice with NAC to decrease the ROS levels markedly increased the prostate weights and tumor growth (Figure 3H). All NAC treated mice had carcinoma with the majority of mice (75%) displaying invasive carcinoma and 25% microinvasive carcinoma (Table 1 and Figure 3-figure supplement 3). The results indicate that high ROS levels are an impediment to tumor progression. Next, we wanted to know whether the efficacy of such a treatment was greater if the mice were treated at a younger age. Therefore the mice were treated at 2 months according to the protocol depicted in Figure 4A. One cohort of mice was sacrificed at 6 months, and another cohort of mice was left untreated for another 6 months and sacrificed at 12 months. A third cohort of mice was used to determine survival. As shown in Figures 4B and Figure 4-figure supplement 1, the treatments did not affect the body weights but significantly reduced the prostate weights of the *Pbsn-Cre4;Pten*$^{f/f}$ mice at the 6-month time point. Analysis of tumor sections at 6 months again showed a marked decrease in cell proliferation and a marked increase

in cell death with the combination of PEITC and rapamycin treatment (Figures 4C-E). Strikingly, the effect of PEITC and rapamycin was sustained even in the cohort of mice that were left untreated for another six months (Figures 4F-I). Interestingly, we found that BrdU incorporation was still decreased (Figure 4H), and cell death was increased (Figure 4H). Finally, treatment with PEITC and rapamycin profoundly increased survival, even though the treatment was stopped at 6 months of age (Figure 4J). Taken together the results suggest that treatment with rapamycin and PEITC not only attenuate prostate tumor growth but also regresses tumor progression.

HK2 expression is induced in Pten-deficient prostate cancer in an Akt-dependent manner

Hexokinases catalyze the first committed step of glucose metabolism by phosphorylating glucose. Hexokinase 2 (HK2), which is not expressed in most mammalian tissues, is markedly induced in cancer cells by different mechanisms (Patra & Hay, 2013, Patra, Wang et al., 2013). Previously, we showed that systemic deletion of HK2 in mice is well tolerated and a therapeutic for lung cancer (Patra et al., 2013). HK2 is also directly phosphorylated by Akt which increased its binding to mitochondria (Miyamoto et al., 2008), and therefore its activity (DeWaal et al., 2018). We therefore examined the human prostate cancer cell lines DU145, PC3 and LNCaP for the expression of HK2 and found that the PTEN-deficient PC3 and LNCaP cells expressed higher levels of HK2 compared with the PTEN-proficient DU145 cells (Figure 5A and Figure 5-figure supplement 1). The high level of HK2 in the PC3 and LNCaP cells was dependent on Akt because treatment with the pan-Akt inhibitor MK2206 diminished HK2 expression (Figure 5A) and because the knockdown of Akt1 and Akt2 in PC3 cells decreased HK2 expression (Figure 5-figure supplement 2). In addition the knockdown of PTEN in DU145 cells increased HK2 expression whereas the expression of PTEN in PC3 and LNCaP cells decreased HK2 expression (Figure 5-figure supplement 3). The knockdown of HK2 only modestly decreased the total hexokinase activity in DU145 cells, while in PC3 and LNCaP cells, HK2 knockdown decreased most of the total hexokinase activity (Figures 5B and 5C). The results suggest that in the PTEN-deficient PC3 and LNCaP cells, HK2 is the major contributor of hexokinase activity. Indeed the knockdown of hexokinase 1 (HK1) in PC3 cells had only a modest effect on the total hexokinase activity (Figure 5-figure supplement 4) and no effect on cell proliferation in comparison with HK2 knockdown (Figure 5-figure supplement 5).

HK2 deficiency in Pten-deficient prostate cancer cells impairs proliferation and tumorigenesis and overrides chemoresistance

HK2 knockdown in PC3 and LNCaP cells markedly affected the proliferation of the cells, as measured by the cell numbers and BrdU incorporation, whereas the proliferation of the DU145 cells was not significantly affected (Figures 5D-E). The knockdown of HK1, however, did not affect the proliferation of PC3 cells and did not further decrease the attenuated proliferation induced by HK2 knockdown (Figure 5-figure supplement 5). Furthermore, the knockdown of HK2 impaired the anchorage-independent growth of PC3 cells (Figure 5F). PTEN-deficient prostate cancer cells are relatively resistant to etoposide because of Akt activation (Figure 5-figure supplement 6). However, HK2 knockdown re-sensitizes these cells to death induced by etoposide (Figure 5G). The inducible knockdown of HK2 in PC3 cells in nude mice after tumor onset substantially decreased tumor growth. Etoposide alone also inhibited tumor growth, although to a lesser extent. However, the combination of HK2 knockdown and etoposide prohibited tumor growth by both decreased proliferation and increased cell death (Figure 5H and Figure 5-figure supplement 7). Finally, we observed that glycolysis, as measured by ECAR, was significantly reduced in PC3 cells after HK2 knockdown as expected (Figure 5-figure supplement 8), but this was associated with a compensatory increase in oxygen consumption (OCR) (Figure 5-figure supplement 9). Consequently, the ROS levels were further increased in PC3 cells (Figure 5-figure supplement 10), and therefore, the cells became more sensitive to PEITC-induced cell death (Figure 5-figure supplement 11These results suggest that HK2 depletion together with PEITC could be an additional therapeutic strategy for PTEN-deficient prostate cancer cells.

Hk2 deletion in *Pbsn-Cre4;Pten$^{f/f}$* mice inhibits prostate tumor development by decreasing proliferation and increasing cell death

To further address the role of HK2 in prostate neoplasia *in vivo*, we crossed *Pbsn-Cre4;Pten$^{f/f}$* mice with *Hk2$^{f/f}$* mice to generate *Pbsn-Cre4;Pten$^{f/f}$;Hk2$^{f/f}$* mice. As shown in Figure 6A, HK2 expression was induced in the prostates of *Pbsn-Cre4;Pten$^{f/f}$* mice compared with that of the control mice. The deletion of HK2 in the *Pbsn-Cre4;Pten$^{f/f}$;Hk2$^{f/f}$* mice markedly decreased the prostate weights (Figure 6B) and substantially increased the survival compared with those of the

Pbsn-Cre4;Pten$^{f/f}$ mice (Figure 6C). Analysis of the prostate tumor sections showed that HK2 deletion not only inhibited tumor proliferation, as measured by BrdU incorporation, but also significantly increased apoptosis, as measured by caspase-3 cleavage Figures 6D and E). We concluded that HK2 is required for prostate cancer development and that its deletion induces both cytostatic and cytotoxic effects.

Discussion

Akt is frequently hyperactivated in human cancers. However, systemic pan-Akt inhibition could also exert toxicity and undesired effects, such as hyperinsulinemia, hyperglycemia, liver injury, and inflammation (Wang et al., 2017). Therefore, alternative therapeutic approaches that can selectively target cancer cells with hyperactive Akt are highly desired. Akt activation induces metabolic changes that can be exploited to selectively target cancer cells displaying hyperactive Akt. Akt is frequently hyperactivated in prostate cancer due to loss of the tumor suppressor PTEN. We therefore exploited the metabolic consequences of Akt activation in PTEN-deficient prostate cancer. Akt activation in PTEN-deficient prostate cancer elevates oxygen consumption and intracellular ROS levels. Since Akt activation cannot protect cells against ROS-induced cell death, the high level of ROS mediated by Akt activation renders cells with hyperactive Akt more vulnerable to ROS-induced cell death. Rapamycin further induced Akt activity by inhibiting the feedback inhibition of Akt by mTORC1(Nogueira et al., 2008). Since treatment with rapamycin further increased ROS-induced cell death, we combined a ROS inducer with rapamycin as a therapeutic approach to eradicating the PTEN-deficient prostate tumors of human xenografts in mice and in a mouse model of prostate neoplasia. This therapeutic approach also converts the cytostatic effect of rapamycin to a cytotoxic effect. This strategy was successful in eradicating prostate tumors in vivo. In the mouse model of Pten-deficient prostate cancer, we found that this strategy inhibited prostate tumor growth, which was sustained even six months after the treatment was stopped. Interestingly six months after the treatment was stopped not only we observed inhibition of proliferation but continuous increase in cell.

High ROS levels in cancer cells can contribute to tumorigenesis and promote pro-oncogenic signaling. However, high ROS levels could also be impediment to tumor progression and metastasis (Le Gal, Ibrahim et al., 2015, Piskounova, Agathocleous et al., 2015, Sayin, Ibrahim et al., 2014). Indeed, we found that in contrast to treatment with a ROS inducer,

treatment with a ROS scavenger increased tumor development and invasiveness in *Pbsn-Cre*; *Pten*$^{f/f}$ mice.

We found that high level of glycolysis in PTEN-deficient prostate cancer cells is partially dependent on the ability of Akt to elevate HK2 expression. HK2 expression was not detected in the prostates of normal mice but was markedly induced after the deletion of PTEN in the prostates. In addition, HK2 is phosphorylated by Akt and increases the binding of HK2 to mitochondria (Miyamoto et al., 2008, Roberts, Tan-Sah et al., 2014). Because the binding of HK2 to mitochondria increases glycolysis (DeWaal et al., 2018), Akt likely not only increases HK2 expression but also increases its activity in PTEN-deficient prostate cancer. HK2 knockdown in Pten-deficient prostate cancer cells in mice markedly inhibited their tumor growth and overcame their resistance to etoposide. The deletion of HK2 in the prostates of *Pbsn-Cre4;Pten*$^{f/f}$ mice inhibited tumor growth and markedly extended their survival. Interestingly, unlike in other mouse models of cancer (Patra et al., 2013), HK2 deletion in the prostate of *Pbsn-Cre*; *Pten*$^{f/f}$ mice is not only cytostatic but also cytotoxic.

In adult mice, HK2 is not expressed in most tissues, and high expression of HK2 is limited to a small number of normal tissues (Patra & Hay, 2013, Patra et al., 2013). However, HK2 expression is markedly elevated in cancer cells. Since systemic HK2 deletion is tolerated in mice, HK2 inhibition is a viable approach to circumvent chemoresistance induced by Akt activation in prostate cancer. Furthermore, it was recently demonstrated that it is feasible to develop inhibitors that preferentially inhibit HK2 and not HK1 (Lin, Zeng et al., 2016). In summary, we provided two therapeutic approaches exploiting the increased OXPHO and glycolysis levels by Akt to selectively eradicate PTEN-deficient prostate cancer.

Materials and Methods

Cell lines

The DU145, PC3, LNCaP, 293FT and phoenix cells were purchased from ATCC. The DU145, PC3, and LNCaP cells were maintained in RPMI-1640/10% FBS/1% pen-strep media. The 293FT and phoenix-amphotropic cells were maintained in DMEM/10% FBS/1% pen-strep media. All cells were maintained in the exponential phase of growth at 37°C in a humidified 5% CO_2 atmosphere. Tet-free FBS was used to maintain the Tet-ON HK2sh and Tet-ON control

(shScr) cells in the absence of doxycycline, and doxycycline induction was at 900ng/mL for the inducible DU145, PC3 and LNCaP HK2 knockdown cell lines.

All cells were confirmed to be mycoplasma negative, using the Sigma LookOut Mycoplasma PCR Detection Kit.

Retrovirus and lentivirus production and infection

pBabe-Puro-PTEN-HA was previously described by Furnari *et al*.(Furnari, Lin et al., 1997). pBabe-Puro-mAkt was previously described in (Kennedy, Kandel et al., 1999). Human PTEN was targeted in DU145 cells with an shRNA (5'-ACTTGAAGGCGTATACAGGA-3') cloned into the pLenti6 lentiviral vector using the BLOCK-iT Lentiviral Expression System (Thermo Fisher scientific). The sequences of the shRNAs targeting Akt1 and Akt2 to generate the PC3 Akt1/Akt2 double knockdown cells were described in (Nogueira et al., 2008). The sequences of the shRNAs targeting human HK2 (HK2 shRNA3) used in this study were described in (Patra et al., 2013). The pLKO.1 lentiviral vector containing human HK1 shRNA from Sigma was used (stock # TRCN0000037656).

Amphotropic retrovirus production was performed as previously described (Skeen, Bhaskar et al., 2006). Lentiviruses were made in 293FT cells using the virapower lentiviral system (Invitrogen) according to the manufacturer's protocol. Viruses were collected 40-50 h after transfection, and target cells were incubated with virus for 24 h in the presence of polybrene (8 μg/ml). Cells were selected using 9 μg/ml blasticidin, 1.3 μg/ml puromycin or 0.2 mg/ml zeocin for 4-6 days, and a mock infection plate was used as a reference. Cells were expanded for two passages in drug-free media and frozen for subsequent use. Early passage cells were used for every experiment.

siRNA Transfection

SMARTpool ON-TARGET plus SESN3 and control non-targeting siRNA were purchased from Dharmacon. DU145 (8×10^4 cells/well) cells were plated in 6-well plates in DMEM supplemented with 10% FBS. The next day, cells were transfected with 50 nM control-siRNA or sestrin3-siRNA using DharmaFECT reagent (Dharmacon) according to the manufacturer's instructions. Cells were split for ROS measurement or treatment with PEITC followed by

assessment of cell death 72 h after transfection.. The knockdown efficiency was analyzed by either immunoblotting or real-time PCR.

Immunoblot analysis

For western blot analysis, $2x10^6$ cells were plated on 10-cm plates and allowed to grow for 24 h. The cells were then treated as described in the figure legends or harvested in PBS, and cell pellets were washed and frozen at -80°C. Cell extracts were then made using ice-cold lysis buffer [20 mM Hepes, 1% Triton X-100, 150 mM NaCl, 1 mM EDTA, 10 mM sodium pyrophosphate, 100 mM NaF, 5 mM iodo-acetic acid, 20 nM okadaic acid, 0.2 mM phenylmethylsulfonyl fluoride and a complete protease inhibitor cocktail tablet (Thermo Fisher)]. For the tissue extracts, frozen tissues collected by liquid nitrogen snap freezing were thawed and homogenized in the same buffer. The extracts were run on 6 to 12% SDS-PAGE gels, transferred to PVDF membranes, and probed with the following antibodies: anti-phospho-Akt Ser473, anti-panAkt, anti-cleaved caspase-3, anti-HK1, anti-HK2 anti-PTEN (Cell Signaling Technology), anti-HA (Covance), anti-4HNE (JaICA), anti-catalase, anti-CuZnSOD and anti-MnSOD (StressGen), anti-SESN3 (ProteinTech) and anti-ß-actin (Sigma). Immunoblots were quantified using the NIH ImageJ software program by densitometric signal and normalized as described in figure legends.

Cell death assays

Cells were treated as described in the figure legends, and apoptosis and cell death was quantified by DAPI staining as previously described **(Kennedy et al., 1999)** or by PI staining as previously described **(Nogueira et al., 2008)**. For DAPI staining, 13% formaldehyde was added directly to medium. After 17h, media was removed and DAPI solution (1mM in PBS) added to plates. Cells were then rinsed with PBS and visualized with immunofluorescence microscope. At least 5 fields per plates were scored for percentage of apoptotic cells. For quantification of apoptosis by cleaved caspase3/7 assay, cells (15×10^3/well) were plated in a 48 - well plates. Upon treatment to induce cell death, NucView-conjugated Caspase - 3 substrate (Nexcelom ViaStain™ Live Caspase 3/7 Detection) was also added at a final concentration of 4μM. During apoptosis, caspase 3/7 proteins cleave its substrate complex and thereby release the high-affinity DNA dye (NucView), which translocates to the nucleus and binds to the DNA, producing a bright green fluorescent signal. Thirty minutes before the end of the incubation, Hoechst 33342 is added to

each well (4μg/ml) and fluorescence was measured with the Celigo Image Cytometer. The percentage of Green (apoptotic) to Total (Blue-Hoechst) is calculated.

Measurement of ROS

Intracellular ROS generation was assessed using 2',7'-dichlorofluorescein diacetate or dihydroethidium (Molecular Probes) as described in (Nogueira et al., 2008).

NADPH and GSH assays

The intracellular levels of NADPH and total NADP (NADPH+$NADP^+$) were measured with previously described enzymatic cycling methods, as described in (Jeon, Chandel et al., 2012). The intracellular levels of GSH and total glutathione (GSSG + GSH) were measured with the use of enzymatic cycling methods, as described previously (Rahman, Kode et al., 2006).

Oxygen consumption assay

For the oxygen consumption measurement, two instruments were used, a Clark-type oxygen electrode and an XF96e Extracellular Flux analyzer (Agilent Seahorse). For the Clark-type oxygen electrode method, $2x10^6$ cells were plated and cultured overnight. Cells were then harvested, washed with PBS and resuspended in 500 μl of fresh RPMI. The rate of oxygen consumption was measured at 37°C using a Strathkelvin Model 782 oxygen meter equipped with a Clark-type oxygen electrode. The results are expressed as the nanomoles of oxygen consumed per minute and per million cells. For the Agilent Seahorse method, see below.

Mitochondrial Membrane Potential

MMP was determined with JC-1 dye (Thermofisher) using FACScan flow cytometer. JC-1 dye accumulates in the mitochondrial membrane in a potential-dependent manner. High potential of the inner mitochondrial membrane facilitates formation of the dye aggregates with both excitation and emission shifted towards red light when compared with that for JC-1 monomers (green light). Cells were seeded into 12-well black plate at a density of 10×10^4cells/well, trypsinized and resuspended in JC-1 solution (10μg/ml) in RPMI and incubated in CO_2 incubator at 37°C for 30 min. Before measurements, the cells were centrifuged and then washed twice with the PBS and immediately analyzed by flow cytometry. Each experiment included a positive

control; 10μM of the FCCP was added to the cells as an uncoupler. Results are shown as a ratio of fluorescence measured with red to green filters (aggregates to monomer fluorescence). Each sample was run three times in triplicate.

Measurement of the oxygen consumption rate (OCR) and the extracellular acidification rate (ECAR)

OCR and ECAR measurements were performed using the XF96e Extracellular Flux analyzer (Agilent Technologies, Santa Clara, CA). Cells were plated on XF96 cell culture plates (Agilent Technologies) at $3x10^4$ cells per well. The cells were incubated for 24 h in a humidified 37°C incubator with 5% CO_2 in RMPI-1640 medium (10% FBS). One hour prior to performing an assay, the growth medium in the wells of an XF cell plate was replaced by XF assay medium (XF base medium lacking bicarbonate and HEPES containing 10 mM glucose, 1 mM sodium pyruvate and 2 mM glutamine for OCR measurements and 2 mM glutamine only for ECAR measurements), and the plate was transferred to a 37°C CO_2-free incubator. For OCR measurement, successive injection of compounds measured ATP-coupled respiration (1 μM oligomycin), maximal respiration (0.5 μM FCCP) and non-mitochondrial respiration (0.5 μM rotenone/antimycin A). Basal respiration, proton leakage and spare respiratory capacity were then calculated using these parameters. For ECAR measurement, successive injection of compounds measured glycolysis (10 mM glucose), glycolytic capacity (1 μM oligomycin) and non-glycolytic acidification (50 mM 2-deoxyglucose). The glycolytic reserve was then calculated using these parameters. In a typical experiment, 3 baseline measurements were taken prior to the addition of any compound, and 3 response measurements were taken after the addition of each compound. The OCR and ECAR are reported as being normalized against cell counts (pmoles/min/10^6 cells for OCR and mpH/min/10^6 cells for ECAR). The baseline OCR or ECAR refers to the starting rates prior to the addition of a compound. Each experiment was performed at least 3 times in triplicate.

HK Activity

Whole-cell HK activity was measured as described previously (Majewski, Nogueira et al., 2004).

Cell proliferation and BrdU incorporation

Cells (4x 10^4) were plated on 6-cm dishes in triplicate and counted every day for 6 days. Media was changed on the third day to ensure continuous natural growth. For BrdU incorporation, on the third day of proliferation, a subset of cells was pulsed with 3 μg/mL BrdU for 2 h and fixed with 70% ethanol. In addition, immunostaining was performed with primary anti-BrdU monoclonal antibodies (Dako) followed by a FITC-conjugated secondary antibody.

Anchorage independent growth assay

In brief, cells (20×10^3) were re-suspended in a single cell suspension in 10% FBS in RPMI medium containing 0.35% agarose and plated onto a layer of 0.7% low-melt agarose-containing medium in a 6-well dish. Cells were grown for 3 weeks in media, and doxycycline was replaced every three days. Soft-agar colonies from the entire well were counted after 3 weeks. The experiments were performed three times in triplicate.

Real-Time PCR and Primers

Total RNA was extracted using TRIzol reagent (Invitrogen), and first strand cDNA was produced with SuperScript III reverse transcriptase (Invitrogen) following the standard protocol. Quantitative PCR was performed with BIO-RAD iQ-SYBR green super-mix and the related system. Samples were assayed in triplicate, and data were normalized to the actin mRNA levels. The primer sequences for hSesn3 were 5'- ATG CTT TGG CAA GCT TTG TT -3' and 5'- GCA AGA TCA CAA ACG CAG AA -3', and the primer sequences for hActin were 5'-CCA TCA TGA AGT GTG ACG TGG -3' and 5'-GTC CGC CTA GAA GCA TTT GCG -3'.

Mice strains and husbandry

All mice in this study were from C57BL/6 background. The *Pbsn-Cre4;Pten$^{f/f}$* mice were described previously. *Pbsn-Cre4;Pten$^{f/+}$* mice were intercrossed to generate the following genotypes for experiments: *Pten$^{f/f}$, Pbsn-Cre4, Pten$^{f/f}$* and *Pbsn-Cre4;Pten$^{f/f}$;Hk2$^{f/f/}$* were described in **(Patra et al., 2013)**. *Hk2$^{f/f}$* and *Pbsn-Cre4;Pten$^{f/f}$* mice were intercrossed to obtain mice with the following genotypes: *Pbsn-Cre4;Pten$^{f/f}$;Hk2$^{f/f}$* and *Pten$^{f/f}$;Hk2$^{f/f}$* which were used for experiments. All animal experiments were approved by the University of Illinois at Chicago institutional animal care and use committee.

Xenograft studies

Male athymic mice (6 to 8 weeks old) were purchased from Charles River Laboratories and maintained in accordance with the NIH Guide for the Care and Use of Laboratory Animals. Cells (PC3 or DU145, 2 x 10^6/0.1 ml PBS) were injected subcutaneously into both the left and right flanks of each mouse. The mice were equally randomized into different treatment groups (see the figure legend). When the tumors reached a size of 10 to 15 mm^3, the animals were treated with the indicated drugs (35 mg/kg PEITC, 2 mg/kg rapamycin, and a combination of rapamycin/PEITC (1:1)) from Monday through Friday by intraperitoneal injection. All the drugs were dissolved in solvent containing ethanol, cremophor-EL (Sigma), and PBS (1:1:8 volume ratio). Control mice were injected with an equal volume of solvent as a control. The body weights and tumor sizes of the mice were measured and recorded twice per week for the duration of the experiment. When the tumor sizes reached the end-point criterion (e.g., a diameter greater than 2 cm), the mice were euthanized, and xenograft tumors were collected. Tumor tissues from representative mice from each group were sectioned, embedded in paraffin, and stained.

For the doxycycline inducible experiments, PC3 Tet-ON HK2sh cells (2×10^6 in 0.1 ml of PBS) expressing doxycycline-inducible shRNA constructs were subcutaneously injected into male nude mice. Once tumors were palpable, the mice were randomly assigned into different groups and fed regular chow (control) or doxycycline chow (200 mg/kg of diet (Bio_Serv)), and they received an IP injection of the vehicle solvent etoposide (10 mg/kg) as described above.

Prostate tumor development and survival curves

Control and *Pbsn-Cre4;Pten*$^{f/f}$ mice were treated with vehicle, rapamycin, PEITC or a combination of rapamycin/PEITC at the same doses described above at 2 different ages, 2 and 4 months. A schematic and the frequency of treatment are described in the figure legends. At the end of the study, prostate tissues will be collected for immunoblot analysis (snap-freezing in liquid nitrogen) or histopathology (formalin fixation).

For the NAC study, a subset of four-month-old control and *Pbsn-Cre4;Pten*$^{f/f}$ mice received a daily (5 days a week) intraperitoneal injection of N-acetyl-cysteine (200mg/kg, pH 7.4 in PBS) or PBS for 12 consecutive weeks. At the end of the study, tissues will be collected for immunoblot analysis (snap-freezing in liquid nitrogen) or histopathology (formalin fixation).For

the survival curve experiments, the mice were monitored until their death or until humane end-point criteria was attained (e.g., distended abdomens).

Histopathology and immunohistochemistry.

Xenograft tumors (nude mice) and prostate tissues were collected at the indicated time points, rinsed in PBS, and quickly fixed in 10% formalin overnight before being subsequently preserved with 70% ethanol. The fixed tissues were then processed and embedded in paraffin. The paraffin embedded tissues were processed, and 5 μM slides were prepared for hematoxylin and eosin (H&E) staining or immunostaining. For antigen retrieval, tissue sections were incubated at 95°C in 10 mM citric acid (pH 6.0) for 30 min. Detection was achieved using ABC-DAB kits (Vector Laboratories), an anti-BrdU mouse monoclonal antibody (Dako# M0744), and an anti-cleaved caspase-3 (Asp175) antibody (Cell Signaling). For quantification, cells were counted from 4 section fields at a 40x magnification using four mice per condition.

BrdU incorporation in mice

For the BrdU labeling experiments, mice were injected intraperitoneally with BrdU (Sigma) in PBS (0.5 mg BrdU/10 g of body weight) 2 h prior to sacrifice and tissue collection. Tumors were collected and processed as described above. After dewaxing and rehydration, paraffin sections were digested by pepsin followed by EcoRI and Exonuclease III. The slides were then incubated with anti-BrdU and processed for immunohistochemistry as described above.

Statistical analysis

Statistical analysis was performed using unpaired Student's t-tests. Survival curves were analyzed by log-rank tests, and the data are expressed as the mean ±SEM as indicated in the figure legends. Unless otherwise indicated, all the experiments were performed at least three times in triplicate.

Acknowledgements

This work was supported by the ACS-IL grant 09-30 to V.N, the NIH grants R01AG016927, R01 CA090764, and R01 CA206167, and the VA merit award BX000733 to N.H.

Competing financial interests

There are no competing financial interests.

Table 1

	Grade				
	No PIN	**Low Grade PIN**	**High Grade PIN**	**Microinvasive Carcinoma**	**Invasive Carcinoma**
Pbsn-Cre4;Pten$^{f/f}$ *			66%	33%	
Pbsn-Cre4;Pten$^{f/f}$ **R+P** **	33%	16%	33%	16%	
Pbsn-Cre4;Pten$^{f/f}$ **+NAC** ***				25%	75%

* The anterior lobes of prostates from untreated mice were analyzed by histopathology at 8 months (Percentage of mice with highest grade is indicated).

** The anterior lobes of prostates from mice treated at 4 months with rapamycin and PEITC (R+P) were analyzed by histopathology at 8 months (Percentage of mice with highest grade is indicated).

*** The anterior lobes of prostates from mice treated at 4 months with NAC were analyzed by histopathology at 8 months (Percentage of mice with highest grade is indicated).

641

642 **Figure legends**

643 **Figure 1: Akt activation in PTEN-deficient prostate cancer cells elevates oxygen**
644 **consumption and intracellular ROS levels.** The human CaP cells DU145, PC3 and LNCaP
645 were seeded in 10% FBS and harvested after two days to measure various parameters.
646 (A)Immunoblot showing the expression levels of PTEN, P-Akt (ser 473), pan-Akt and ß-actin as
647 a loading control. (B) Oxygen consumption: OCR was measured using the Seahorse XF96^{e}
648 analyzer for all three CaP cell lines. After the OCR was established, oligomycin (1), FCCP (2)
649 and rotenone/antimycin A (3) were added sequentially. The traces shown are representative of
650 three independent experiments in which each data point represents technical replicates of four
651 wells each ± SEM. (D, E) Relative ROS levels: CaP cells were incubated with H2DCFDA (D) or
652 DHE (E), and the levels of fluorescence were analyzed by flow cytometry as an indicator of ROS
653 levels. Data represent the mean ± SEM of three independent experiments performed in triplicate.
654 *p < 0.01, ***p < 0.005 versus DU145. No significant differences between PC3 and LNCaP
655 were observed. (C, F) Akt1 and Akt2 were knocked down in PC3 cells, and the OCR (C) and
656 cytosolic ROS levels (F) were measured. The results are presented as the average of at least three
657 independent experiment performed in triplicate ± SEM. ###p < 0.0001 versus PC3 LacZsh.
658 Insert in (C) shows the expression levels of Akt1, Akt2 and ß actin as a loading control in PC3
659 cells in which Akt1 and Akt2 were knocked down.

660

661 **Figure 2: ROS inducers and the combination of a ROS inducer and rapamycin induce CaP**
662 **PTEN-deficient cell death in vitro and eradicate their tumors in vivo.**
663 (A) CaP cell lines were incubated with 2-ME for 24 h, the cells were fixed and apoptosis was
664 quantified by DAPI staining. The data represent the mean ± SEM of three independent
665 experiments performed in triplicate. *p < 0.005, **p < 0.002 versus DMSO (0 μM) for each cell
666 line. #p < 0.02, ##p < 0.01 versus DU145. (B) CaP cell lines were incubated with PEITC,
667 collected and fixed for estimation of cell death by PI staining or lysed to extract total protein.
668 They were then subjected to immunoblotting with cleaved caspase-3 and ß-actin as a loading
669 control (insert). The data represent the mean ± SEM of three independent experiments performed
670 in triplicate. *p < 0.005, ***p < 0.001 versus DMSO for each cell line. ###p < 0.0005 versus
671 DU145. (C) PC3 Akt1/2 knockdown cells were incubated with PEITC for 17 h, and then cell

672 death was estimated by PI staining as the percentage of apoptotic cells among total cells. The
673 data represent the mean ± SEM of three independent experiments performed in triplicate. **p <
674 0.001, ***p < 0.0001 versus DMSO for each cell line. ##p < 0.005, ###p < 0.0001 versus PC3
675 LacZsh. (D) CaP cells were incubated for 8 h with 20 nM rapamycin (RAPA) prior to the
676 addition of PEITC (3 μM). After 17 h of incubation with PEITC, the cells were fixed, and
677 apoptosis was quantified by DAPI staining. The data represent the mean ± SEM of three
678 independent experiments performed in triplicate. ***p < 0.0001 versus PEITC for each cell line.
679 ##p < 0.0005 versus DU145. (E- H) In vivo therapeutic effect of rapamycin + PEITC in mice
680 inoculated with PC3 prostate cancer cells. Thirty-two nude mice were subcutaneously injected
681 with PC3 cells in both flanks and randomly divided into four groups (8 mice per group, 16
682 tumors per group) for treatment with PEITC, rapamycin (RAPA), a combination of RAPA +
683 PEITC, or a solvent control (Vehicle). (E) Graph presenting the tumor growth rates in each
684 group. Treatment began on day 13 (~15 mm^3, red arrow) and stopped on day 43 after tumor cell
685 inoculation. The data represent the average size ± SEM of 16 tumors up to day 43. The data
686 collection from day 57 average the size of the 8 remaining xenograft tumors only. *p < 0.003,
687 **p < 0.002 versus vehicle. #p < 0.03, ##p < 0.01 versus PEITC or RAPA. (F) Cross-sections of
688 tumors collected from the experiment described in (E). At day 50 after tumor cell inoculation,
689 the tumor cross-sections were subjected to hematoxylin and eosin (H & E, top) staining, BrdU
690 staining (middle), and anti-cleaved caspase-3 staining (bottom). Scale bars: 100 μm. (G, H)
691 Histograms showing quantification of the positively stained cells in (F). The results are presented
692 as the mean ± SEM of the positively stained cells of four sections from four treated mice. The
693 stained cells were counted in four random fields of each section. ***p < 0.0002 versus vehicle.
694 ##p < 0.001 versus PEITC.
695
696 **Figure 3: The effect of rapamycin, PEITC and the combination of rapamycin and PEITC**
697 **on cell proliferation, cell death, survival and the tumors of *Pbsn-Cre4;Pten$^{f/f}$* mice.** (A)
698 Tissue lysates were prepared from prostates isolated from 4 control mice (*Pten$^{f/f}$* or *Pbsn-Cre4*)
699 and 4 *Pbsn-Cre4;Pten$^{f/f}$* mice. Immunoblot analysis shows the expression levels of PTEN, Akt-P
700 (ser 473), total-Akt, p21, 4HNE and ß-actin as a loading control. (B) Schematic of mouse
701 treatment: control (*Pten$^{f/f}$* or *Pbsn-Cre4*) and *Pbsn-Cre4;Pten$^{f/f}$* mice were randomly divided into
702 four groups of 9 to 16 mice at 4 months of age, and they received a daily (5 days a week)

intraperitoneal injection of drugs, PEITC (35 mg/kg BW), rapamycin (2 mg/kg BW), rapamycin in combination with PEITC (1:1) or solvent control, for 6 consecutive weeks. Treatment was then interrupted for 3 weeks and resumed at 6 months of age for another 6 weeks. The mice were sacrificed at 8 months of age and examined for the presence of prostate hyperplasia. (C) Graphs showing the relative prostate weight to total body weight (% body weight) of *Pbsn-Cre4;Pten*$^{f/f}$ mice treated with vehicle (n=15 mice), rapamycin (RAPA, n=11), PEITC (n=9) or RAPA+PEITC (n=16). The box plots represent the 25th to 75th percentiles (boxes) with the median, and the whiskers represent the maximum and minimum values. *p=0.05, **p=002, ***p < 0.0001 versus vehicle. ###p < 0.0005 versus PEITC. (D) The cross-sections of prostate tissues collected at 8 months from *Pbsn-Cre4;Pten*$^{f/f}$ mice treated with different drugs were subjected to H & E staining (top), BrdU staining (middle), and anti-cleaved caspase-3 staining (bottom). Scale bars: 100μm (E-F) Histograms showing quantification of the positively stained cell cross-sections shown in Figure 3D for BrdU (E) and cleaved caspase-3 (F). The results are presented as the mean ± SEM of positively stained cells of four sections from four treated mice. The stained cells were counted in four random fields of each section. *p<0.002, **p < 0.005, ***p < 0.0002 versus vehicle. #p=0.04, ##p=0.01 versus PEITC. (G) A cohort of 20 *Pbsn-Cre4;Pten*$^{f/f}$ mice treated with vehicle (n=10) or rapamycin in combination with PEITC (R+P; n=10) were kept alive, and Kaplan-Meier curves of the percentage of mice survival is shown. The vehicle-treated mice have a medium survival age of 322 days versus 443 days for the 'R+P' treated mice. The p-values and median survival were calculated by log-rank tests. (H) Graph showing the relative prostate weights of *Pbsn-Cre4;Pten*$^{f/f}$ mice (n=15) treated with N-acetyl-cysteine (NAC, n=9) or PBS (n=6) at 8 months of age and 11 *Pten*$^{f/f}$ mice (NAC, n=7 and PBS, n=4). The data represent the mean ± SEM. **p=0.0006, ***p=0.0001 versus *Pten*$^{f/f}$. #p=0.01, ##p=0.003 versus PBS for each mice genotype.

Figure 4: Early treatment of *Pbsn-Cre4;Pten*$^{f/f}$ mice with rapamycin + PEITC inhibits tumor growth and increases survival, even after treatment was halted for six months.

(A) Schematic of mice treatment: control and *Pbsn-Cre4;Pten*$^{f/f}$ mice were randomly divided into four groups of 4 to 10 mice at 2 months of age, and they received IP drug injections as indicated in the schematic. A pool of mice was sacrificed at 6 or 12 months of age and examined for the presence of prostate hyperplasia. (B) Graphs showing the relative prostate weights of

Pbsn-Cre4;Pten$^{f/f}$ mice sacrificed at 6 months and treated with vehicle (n=9), RAPA (n=4), PEITC (n=4) or RAPA+PEITC (n=8). The box plots represent the 25th to 75th percentiles (boxes) with the median, and the whiskers represent the maximum and minimum values. *p=0.03, **p=0.05, ***p < 0.0001 versus vehicle. #p= 0.05 versus PEITC. (C) Representative cross-sections of prostate tissues were treated as described in Figure 4A and collected from *Pbsn-Cre4;Pten*$^{f/f}$ mice treated with different drugs at 6 months. The sections were subjected to H & E staining (top), BrdU staining (middle), and anti-cleaved caspase-3 staining (bottom). Scale bars: 100µm. (D, E) Histograms showing quantification of the positively stained cell cross-sections for BrdU (D) and cleaved caspase-3 (E). The results are presented as the mean ± SEM of the positively stained cells of four sections from four treated mice. The stained cells were counted in four random fields of each section. *p=0.03, **p<0.001, ***p < 0.0001 versus vehicle. #p < 0.05, ###p<0.0001 versus PEITC. (F) Graphs representing the relative prostate weights of *Pbsn-Cre4;Pten*$^{f/f}$ mice sacrificed at 12 months and treated with vehicle (n=5), RAPA (n=7), PEITC (n=6) or RAPA+PEITC (n=10). The box plots represent the 25th to 75th percentiles (boxes) with the median, and the whiskers represent the maximum and minimum values. *p=0.03, **p=0.05, ***p < 0.0001 versus vehicle. #p < 0.05 versus PEITC. (G) Representative cross-sections of prostate tissues were treated with vehicle or RAPA+PEITC and collected at 12 months from *Pbsn-Cre4;Pten*$^{f/f}$ mice left untreated for 6 months after the initial treatment. The sections were subjected to H & E staining (top), BrdU staining (middle), and anti-cleaved caspase-3 staining (bottom). Scale bars: 50µm for 5X objective (H&E), 100µm for 10X objective. (H, I) Histograms showing quantification of the positively stained cell cross-sections for BrdU (H) and cleaved caspase-3 (I). The results are presented as the mean ± SEM of the positively stained cells of four sections from four treated mice. The stained cells were counted in four random fields from each section. **p=0.003, ***p<0.0001 versus vehicle. (H) A cohort of 30 *Pbsn-Cre4;Pten*$^{f/f}$ mice treated with vehicle (n=15) or rapamycin in combination with PEITC (R+P; n=15) were kept alive, and Kaplan-Meier curves of the percentage of survival of these mice is shown. The vehicle-treated mice have a median survival age of 321 days versus 477 days for the 'R+P' treated mice. The p-values and median survival for the indicated treatments were calculated by log-rank tests.

Figure 5: Depletion of HK2 in PTEN-deficient CaP cells inhibits proliferation, oncogenesis, and tumorigenesis while overcoming chemoresistance.

(A) DU145, PC3 and LNCaP cells were treated with MK-2206 (0.5μM - 24 h) to inhibit Akt. The immunoblot is showing the protein levels of P-Akt, total Akt, HK2 and ß actin as a loading control. (B-G) DU145, PC3 and LNCaP cells expressing an inducible control (Scr) or HK2 shRNA were exposed to 900 ng/ml doxycycline for 5 days for HK2 deletion prior to analysis. (B) Immunoblot showing the protein levels of P-Akt, total Akt, HK2, HK1 and ß actin as a loading control. (C) Graphs depicting the total hexokinase activity in these cells. The data represent the mean ± SEM of three independent experiments performed in triplicate. **p < 0.002, ***p<0.001 versus shScr for each cell line. ##p < 0.001, ###p < 0.0001 versus DU145. (D) Cell proliferation after HK2 deletion in the CaP cell lines. The data represent the mean ± SEM of three independent experiments performed in triplicate. *p=0.02, ***p<0.001 versus shScr for each cell line on day 6. ###p < 0.0005 versus DU145 shHK2 on day 6 (E) BrdU incorporation after HK2 deletion. The data represent the mean ± SEM of three independent experiments performed in triplicate. ***p<0.0001 versus shScr for each cell line. #p < 0.05 versus DU145. (F) Anchorage independent growth (soft-agar): PC3 Tet-ON control (SCR) and HK2-sh cells were plated in 0.35% agarose-containing medium before and after HK2 knockdown with doxycycline as described in the experimental procedures, and they were allowed to grow for approximately 3 weeks with bi-weekly media changes. The bar graphs represent the average quantification of the soft agarose colonies in PC3 cells ± SEM of three independent experiments performed in triplicate. ***p < 0.0005 versus PC3 shScr + Doxycycline. ‡p=0.02 versus PC3 shScr – Doxycycline. ###p < 0.0001 versus PC3 shHK2 – Doxycycline. (G) After HK2 knockdown with doxycycline, cells were treated with etoposide for 24 h before apoptosis was assessed by DAPI staining, which is presented as the percentage of apoptotic cells among total cells. The data represent the mean ± SEM of three independent experiments performed in triplicate. **p < 0.001, ***p < 0.0002 versus DMSO (0 μM) for each cell line. #p < 0.001, ###p < 0.0003 versus shScr. (H) In vivo therapeutic effect of etoposide in mice inoculated with PC3 prostate cancer cells. Twenty-four nude mice were injected subcutaneously with PC3 Tet-ON HK2sh cells in both flanks and randomly divided into four groups (6 mice per group, 12 tumors per group) for treatment with etoposide or solvent control (Vehicle). When the tumors were palpable, 2 groups were provided a doxycycline diet, while the

2 other groups remained on the control diet. Etoposide (or vehicle) treatment was started 3 days after the diet was changed (day 13), and treatment was stopped on day 48 after tumor cell inoculation. The data represent the average size ± SEM of 12 xenograft tumors per group. Statistical analysis from day 52 (end-point): ***p < 0.0001 versus the control diet vehicle. ##p < 0.005 versus the doxycycline diet vehicle.

Figure 6: Deletion of HK2 in the prostates of *Pbsn-Cre4;Pten$^{f/f}$* mice extends survival and inhibits tumor growth by inhibiting proliferation and increasing cell death.

(A) Tissue lysates were prepared from prostates isolated from 3 control mice (*Pten$^{f/f}$;HK2$^{f/f}$*), 3 *Pbsn-Cre4;Pten$^{f/f}$* mice and 3 *Pbsn-Cre4;Pten$^{f/f}$;HK2$^{f/f}$* mice. The immunoblot shows the expression levels of PTEN, Akt-P (ser 473), total-Akt, HK2 and ß-actin as a loading control. (B) Graphs showing the relative prostate weights of control (n=23), *Pbsn-Cre4;Pten$^{f/f}$* (PTEN KO, n=21) and *Pbsn-Cre4;Pten$^{f/f}$;HK2$^{f/f}$* (PTEN-HK2 DKO, n=29) mice. The box plots represent the 25th to 75th percentiles (boxes) with the median, and the whiskers represent the maximum and minimum values. ***p < 0.0001 versus control. ### p < 0.0001 versus PTEN KO. The pictures are representative of macroscopic views of the prostates (delineated by a white dash line) of control (left panel), PTEN KO (middle panel) and (PTEN-HK2 DKO) (right panel) mice. (C) A cohort of 43 PTEN KO and 40 PTEN-HK2 DKO mice were kept alive, and Kaplan-Meier curves of the percentage of survival of these mice is shown. The PTEN KO mice have a media survival age of 305 days versus 453 days for the PTEN HK2 DKO mice. The p-values and median survival for the indicated treatments were calculated by log-rank tests. (D) The cross-sections of prostate tissues collected at 8 months from control, PTEN KO and PTEN-HK2 DKO mice were subjected to hematoxylin and eosin (H & E) staining (top), BrdU staining (middle), and anti-cleaved caspase-3 staining (bottom). (E) Histograms showing quantification of the positively stained cells in (D). The results are presented as the mean ± SEM of the positively stained cells of four sections from four treated mice. The stained cells were counted in four random fields of each section. **p<0.0005, ***p < 0.0001 versus control. ##p < 0.0005, ###p<0.0001 versus PTEN KO.

Figure 1-Figure supplement 1:

Mitochondrial membrane potential measured as JC-1 aggregate to monomer ratio. The data represent the mean ± SEM of three independent quantification experiments performed in triplicate. *p < 0.05 versus DU145.

Figure 1-Figure supplement 2:

Immunoblot showing the expression levels of the detoxifying enzymes catalase, MnSOD and Cu/ZnSOD (ß actin as a loading control) in all three CaP cell lines

Figure 1-Figure supplement 3:

Level of SESN3 mRNA relative to that of actin in CaP cells, as assessed by quantitative RT-PCR. The data represent the mean ± SEM of three independent quantification experiments performed in triplicate. ***p < 0.0001 versus DU145. (1s4-5) DU145 cells were transiently transfected with hSESN3 or control RNAi (Dharmacon), and PC3 cells were transiently transfected with lentivirus expressing hSESN3 or TOPO control 72 h prior to the experiments.

Figure 1-Figure supplement 4:

Immunoblot showing the expression levels of sestrin 3 (SESN3) and ß actin as a loading control.

Figure 1-Figure supplement 5:

Level of ROS, as assessed by flow cytometry, after incubation with H2DCFDA. The data represent the mean ± SEM of three independent experiments performed in triplicate. *p=0.02, **p=0.01 versus the control for each cell line.

Figure 2-Figure supplement 1:

Glutathion levels (Left) and GSH/GSSG ratio (Right) in CaP cells after 8h incubation with DMSO or PEITC 6µM. The data represent the mean ± SEM of two independent experiments performed in duplicate.

Figure 2-Figure supplement 2:

(Left) Apoptosis was measured on live cells by caspase 3/7 activity assay after drug treatment: 2-ME 1µM (14h) or 20nM Rapamycin (5h) followed by 6µM PEITC (8h). The data represent the mean ± SEM of two independent experiments performed in quadruplicate. (Right) Cell death was assessed on fixed cells by DAPI staining after drug treatment: 2-ME 1µM (20h) or 20nM Rapamycin (5h) followed by 6µM PEITC (17h). The data represent the mean ± SEM of three independent experiments performed in triplicate

Figure 2-Figure supplement 3:

CaP cell lines were incubated with BSO (2mM) for 36 and 42 h, the cells were fixed and cell death was quantified by PI staining. The data represent the mean ± SEM of three independent experiments performed in triplicate.

Figure 2-Figure supplement 4:

$NADP^+$/NADPH ratio in CaP cells. The data represent the mean ± SEM of three measurements performed in duplicate.

Figure 2-Figure supplement 5:

After modulation of SESN3 expression, PC3 and DU145 cells where treated with PEITC (0, 3 and 6 μM) for 17 h, the cells were fixed and cell death was assessed by DAPI staining. The data represent the mean ± SEM of three independent experiments performed in triplicate. *$p < 0.05$, **$p < 0.01$ versus the control for each cell line.

Figure 2-Figure supplement 6:

DU145, PC3 AND LNCaP cells were incubated with N-acetylcysteine (100 μM NAC) for 2 h prior to 17 h of incubation with PEITC (6 μM) in the presence of NAC or not. The graphs represent the cell death measured by PI staining (Left) or ROS levels after incubation with H2DCFDA (Right). The data represent the mean ± SEM of three independent experiments performed in triplicate.

Figure 2-Figure supplement 7:

Immunoblot showing the expression of PTEN (and HA-Tag), and ß actin as a loading control after PTEN was downregulated in DU145 cells (1: control shLacZ, 2: shPTEN) or overexpressed in PC3 and LNCaP cells (3: control pBP, 4: pBP-PTEN).

Figure 2-Figure supplement 8: PTEN expression determines the levels of ROS and oxygen consumption

PTEN was downregulated in DU145 cells (1: control shLacZ, 2: shPTEN) or overexpressed in PC3 and LNCaP cells (3: control pBP, 4: pBP-PTEN). (A, B) Relative ROS levels: cells were incubated with H2DCFDA (A) or DHE (B), and the levels of fluorescence were analyzed by flow cytometry as an indicator of ROS levels. (C) Basal oxygen consumption

Figure 2-Figure supplement 9:

Cells were incubated with PEITC or Rapamycin/PEITC for 17h and scored for apoptosis 17 h later by DAPI staining. The data represent the mean ± SEM of three independent experiments

performed in triplicate. *p< 0.05, **p< 0.001 versus the control for each cell line. ##p<0.05 versus PEITC

Figure 2-Figure supplement 10:

mAkt was stably overexpressed in DU145. Cells were then incubated for 17h with PEITC or Rapamycin/PEITC before measurement of relative cytosolic ROS level (Left) or cell death (Right).

Figure 2-Figure supplement 11: ROS levels, and ROS-induced cell death are Akt-dependent.

Akt1 and Akt2 were knocked down in PC3 and LNCaP cells. Once cell lines were established, mAkt was re-expressed in these cells. Cells were incubated with PEITC for 17 h, and then cytosolic ROS levels (A) and cell death estimated by PI staining were measured (B). Another set of cells was incubated with PEITC for 12h to estimate apoptosis by caspase 3/7 activity assay (C) as the percentage of positive cells over total cells. The data represent the mean ± SEM of three independent experiments performed in triplicate.

Figure 2-Figure supplement 12: Rapamycin Elevates Akt Activity

(A-C) DU145 (A), PC3 (B) and LNCaP cells (C) were treated with rapamycin (100nM). Total cell extracts were prepared at different time points as indicated and subjected to immunoblotting with antibodies specific for Akt and p-Akt. (D) quantification of immunoblots showing relative Akt phosphorylation, quantified using the NIH ImageJ software program, and normalized to the densitometric signal for total Akt as a control for protein expression. Values are expressed relative to time 0 and data represent the mean ± SEM of three independent experiments.

Figure 2-Figure supplement 13: Rapamycin increases the ROS levels induced by PEITC.

When required, CaP cells were incubated with 20 nM rapamycin (RAPA) for 8 h before the addition of PEITC (3 μM). After 17 h of incubation with PEITC (± RAPA), the ROS levels in live cells after incubation with H2DCFDA were measured by flow cytometry. The data represent the mean ± SEM of three independent experiments performed in triplicate. *p<0.05, ***p<0.0001 versus DMSO for each cell line. ###p< 0.0005 versus PEITC for each cell line.

Figure 2-Figure supplement 14: Torin, not rapamycin, decreases the OCR and ROS levels in PTEN-deficient CaP cells

PC3 and LNCaP cells were incubated for 8 h with rapamycin (RAPA, 20 nM) or torin (250 nM) before measurement of the OCR (Left) or cytoplasmic ROS levels (Right). The data represent

the mean ± SEM of three independent experiments performed in triplicate. *p<0.05, ***p<0.0001 versus DMSO for each cell line.

Figure 2-Figure supplement 15: In vivo therapeutic effects of rapamycin + PEITC in mice inoculated with DU145 prostate cancer cells.

Twenty-four nude mice were injected subcutaneously with DU145 cells in both flanks and randomly divided into four groups (4 mice per group, 8 tumors per group) for treatment with PEITC, rapamycin (RAPA), a combination of RAPA + PEITC, or a solvent control (Vehicle). The graph represents the tumor growth rate in each group. Treatment began on day 18 (~15 mm3) and stopped on day 55 after tumor cell inoculation. The data represent the average size ± SEM of 8 tumors up to day 57. Data collection on day 64 shows only the average sizes of the 4 remaining xenograft tumors. **p < 0.02 versus vehicle, #p= 0.02 versus RAPA.

Figure 3-Figure supplement 1

Graphs showing the body weights of control (left) and *Pbsn-Cre4;Pten*$^{f/f}$ (right) mice at the end-point (8 months). The number of treated mice in the control group were vehicle (n=6), rapamycin (RAPA, n=12), PEITC (n=8) and RAPA+PEITC (n=8), and the number of treated mice in the *Pbsn-Cre4;Pten*$^{f/f}$ group were vehicle (n=15), RAPA (n=11), PEITC (n=9) and RAPA+PEITC (n=16). No significant differences were detected.

Figure 3-Figure supplement 2

Graphs showing the relative prostate weights of the control mice sacrificed at 8 months. The box plots represent the 25th to 75th percentiles (boxes) with the median, and the whiskers represent the maximum and minimum values. No significant differences were detected.

Figure 3-Figure supplement 3: Representative histopathological images.

Representative images of different prostate tumor grades in the anterior lobe of the prostate of untreated mice (-), rapamycin + PEITC, and NAC treated mice. Each individual image was derived from different individual mice. Scale bars = 200μm for 20X magnification, 500μm for 10X magnification.

Figure 4-Figure supplement 1

(A) Graphs showing the body weights of control (left) and *Pbsn-Cre4;Pten*$^{f/f}$ (right) mice at 6 months. The number of treated mice in the control group were vehicle (n=5), RAPA (n=5),

PEITC (n=5) and RAPA+PEITC (n=7), and the number of treated mice in the *Pbsn-Cre4;Pten$^{f/f}$* group were vehicle (n=9), RAPA (n=4), PEITC (n=4) and RAPA+PEITC (n=8). No significant differences were detected. (B) Graphs showing the relative prostate weights of control mice sacrificed at 6 months (left) and 12 months (right). The box plots represent the 25th to 75th percentiles (boxes) with the median, and the whiskers represent the maximum and minimum values. The number of control-treated mice at 12 months were vehicle (n=4), RAPA (n=4), PEITC (n=4) and RAPA+PEITC (n=8). **p=0.005 versus vehicle.

Figure 5-Figure supplement 1

Total protein was extracted from CaP cells and subjected to immunoblotting with HK1, HK2 and ß actin as a loading control

Figure 5-Figure supplement 2

Expression levels of HK2 and ß actin as a loading control in PC3 cells in which Akt1 and Akt2 were stably knocked down.

Figure 5-Figure supplement 3

Immunoblot showing the expression of HK2 (and ß actin as loading control) in CaP cells where PTEN is either downregulated (DU145) or overexpressed (PC3 and LNCaP)

Figure 5-Figure supplement 4

HK1 was stably knocked down in PC3 cells after HK2 knockdown. The immunoblot shows the expression levels of HK1, HK2 and actin as a loading control in PC3 control, HK1 knockdown, HK2 knockdown, and double HK1 and HK2 knockdown cells. The graph shows the total HK activity in the same cells. The data represent the mean ± SEM of three independent experiments performed in duplicate. *p=0.005, ***p<0.0001 versus PC3 LacZsh ntsh. ###p< 0.0001 versus PC3 LacZsh HK1sh. ‡p=0.01versus PC3 HK2sh ntsh.

Figure 5-Figure supplement 5

Cell proliferation after HK1 and/or HK2 deletion in PC3 cells. The data represent the mean ± SEM of three independent experiments performed in triplicate. ***p<0.0001 versus LacZsh cells on day 6.

Figure 5-Figure supplement 6: Etoposide-induced cell death is Akt-dependent.

(A) After mAkt overexpression, DU145 cells were treated with etoposide for 24 h before cell death was assessed by PI staining on live cells with Celigo Image cytometer (B) Akt1 and Akt2

were knocked down in PC3 and LNCaP cells. Cells were then incubated for 24h with Etoposide before measurement of cell death by PI staining on live cells with Celigo Image cytometer. Data are expressed as the percentage of dead cells among total cells and represent the mean ± SEM of two independent experiments performed in triplicate.

Figure 5-Figure supplement 7: Data analysis for in vivo therapeutic study described in Figure 5H.

(A) Graphs showing the relative xenografts tumor weights of mice treated with Control diet/Vehicle, Control diet/Etoposide, DOX diet/Vehicle and Dox diet/Etoposide. The data represent the average size ± SEM of 12 xenograft tumors per group. *p < 0.05, **p < 0.001 versus control diet vehicle. #p < 0.05 versus DOX diet vehicle. (B) The cross-sections of xenograft tumors collected at end-point (day 52) were subjected to H & E staining, BrdU staining, anti-cleaved caspase-3 staining and HK2 staining (from top to bottom). Scale bars: 100μm. (C, D) Histograms showing quantification of the positively stained cells in (B). The results are presented as the mean ± SEM of the positively stained cells of two sections from six xenograft tumors. The stained cells were counted in three random fields of each section. *p<0.05, ***p < 0.0005 versus the control diet vehicle. ###p < 0.0005 versus DOX diet vehicle.

Figure 5-Figure supplement 8: The effect of HK2 knockdown on ECAR.

PC3 cells expressing an inducible control (Scr) or HK2 shRNA were exposed to 900 ng/ml DOX for 5 days for HK2 deletion before analysis. ECAR was measured after HK2 deletion using the Seahorse XF96e analyzer.

Figure 5-Figure supplement 9 The effect of HK2 knockdown on oxygen consumption.

PC3 cells expressing an inducible control (Scr) or HK2 shRNA were exposed to 900 ng/ml DOX for 5 days for HK2 deletion before analysis. OCR was measured after HK2 deletion using the Seahorse XF96e analyzer.

Figure 5-Figure supplement 10: The effect of HK2 knockdown on ROS levels.

PC3 cells expressing an inducible control (Scr) or HK2 shRNA were exposed to 900 ng/ml DOX for 5 days for HK2 deletion before analysis. Cells were incubated with H2DCFDA, and the level of fluorescence was analyzed by flow cytometry as an indicator of ROS levels after HK2 deletion. The data represent the mean ± SEM of three independent experiments performed in triplicate. ***p<0.005 versus PC3 shScr.

Figure 5-Figure supplement 11: The effect of HK2 knockdown on PEITC-induced cell death.

PC3 cells expressing an inducible control (Scr) or HK2 shRNA were exposed to 900 ng/ml DOX for 5 days for HK2 deletion before analysis. After HK2 knockdown with DOX, cells were treated with PEITC (0, 3 and 6 μM) for 17 h before apoptosis was assessed by DAPI staining, which is presented as the percentage of apoptotic among total cells. The data represent the mean ± SEM of three independent experiments performed in triplicate. *$p < 0.02$, ***$p < 0.0001$ versus PC3 shScr.

References

Bae SH, Sung SH, Oh SY, Lim JM, Lee SK, Park YN, Lee HE, Kang D, Rhee SG (2013) Sestrins activate Nrf2 by promoting p62-dependent autophagic degradation of Keap1 and prevent oxidative liver damage. Cell Metab 17: 73-84

Chen CC, Jeon SM, Bhaskar PT, Nogueira V, Sundararajan D, Tonic I, Park Y, Hay N (2010) FoxOs inhibit mTORC1 and activate Akt by inducing the expression of Sestrin3 and Rictor. Dev Cell 18: 592-604

Chowdhury SK, Raha S, Tarnopolsky MA, Singh G (2007) Increased expression of mitochondrial glycerophosphate dehydrogenase and antioxidant enzymes in prostate cancer cell lines/cancer. Free Radic Res 41: 1116-24

DeWaal D, Nogueira V, Terry AR, Patra KC, Jeon SM, Guzman G, Au J, Long CP, Antoniewicz MR, Hay N (2018) Hexokinase-2 depletion inhibits glycolysis and induces oxidative phosphorylation in hepatocellular carcinoma and sensitizes to metformin. Nature communications 9: 446

Dummler B, Hemmings BA (2007) Physiological roles of PKB/Akt isoforms in development and disease. Biochem Soc Trans 35: 231-5

Furnari FB, Lin H, Huang HS, Cavenee WK (1997) Growth suppression of glioma cells by PTEN requires a functional phosphatase catalytic domain. Proc Natl Acad Sci U S A 94: 12479-84

Gottlob K, Majewski N, Kennedy S, Kandel E, Robey RB, Hay N (2001) Inhibition of early apoptotic events by Akt/PKB is dependent on the first committed step of glycolysis and mitochondrial hexokinase. Genes Dev 15: 1406-18

Hay N (2011) Akt isoforms and glucose homeostasis - the leptin connection. Trends Endocrinol Metab 22: 66-73

Hay N (2016) Reprogramming glucose metabolism in cancer: can it be exploited for cancer therapy? Nat Rev Cancer 16: 635-49

Hollander MC, Blumenthal GM, Dennis PA (2011) PTEN loss in the continuum of common cancers, rare syndromes and mouse models. Nat Rev Cancer 11: 289-301

Jeon SM, Chandel NS, Hay N (2012) AMPK regulates NADPH homeostasis to promote tumour cell survival during energy stress. Nature 485: 661-5

Kennedy SG, Kandel ES, Cross TK, Hay N (1999) Akt/Protein kinase B inhibits cell death by preventing the release of cytochrome c from mitochondria. Mol Cell Biol 19: 5800-10

Kim D, Dan HC, Park S, Yang L, Liu Q, Kaneko S, Ning J, He L, Yang H, Sun M, Nicosia SV, Cheng JQ (2005) AKT/PKB signaling mechanisms in cancer and chemoresistance. Front Biosci 10: 975-87

Kopnin PB, Agapova LS, Kopnin BP, Chumakov PM (2007) Repression of sestrin family genes contributes to oncogenic Ras-induced reactive oxygen species up-regulation and genetic instability. Cancer Res 67: 4671-8

Le Gal K, Ibrahim MX, Wiel C, Sayin VI, Akula MK, Karlsson C, Dalin MG, Akyurek LM, Lindahl P, Nilsson J, Bergo MO (2015) Antioxidants can increase melanoma metastasis in mice. Science translational medicine 7: 308re8

Lin H, Zeng J, Xie R, Schulz MJ, Tedesco R, Qu J, Erhard KF, Mack JF, Raha K, Rendina AR, Szewczuk LM, Kratz PM, Jurewicz AJ, Cecconie T, Martens S, McDevitt PJ, Martin JD, Chen SB, Jiang Y, Nickels L et al. (2016) Discovery of a Novel 2,6-Disubstituted Glucosamine Series of Potent and Selective Hexokinase 2 Inhibitors. ACS Med Chem Lett 7: 217-22

Majewski N, Nogueira V, Bhaskar P, Coy PE, Skeen JE, Gottlob K, Chandel NS, Thompson CB, Robey RB, Hay N (2004) Hexokinase-mitochondria interaction mediated by Akt is required to inhibit apoptosis in the presence or absence of Bax and Bak. Mol Cell 16: 819-30

Mayer IA, Arteaga CL (2016) The PI3K/AKT Pathway as a Target for Cancer Treatment. Annu Rev Med 67: 11-28

Miyamoto S, Murphy AN, Brown JH (2008) Akt mediates mitochondrial protection in cardiomyocytes through phosphorylation of mitochondrial hexokinase-II. Cell Death Differ 15: 521-9

Morita M, Gravel SP, Chenard V, Sikstrom K, Zheng L, Alain T, Gandin V, Avizonis D, Arguello M, Zakaria C, McLaughlan S, Nouet Y, Pause A, Pollak M, Gottlieb E, Larsson O, St-Pierre J, Topisirovic I, Sonenberg N (2013) mTORC1 controls mitochondrial activity and biogenesis through 4E-BP-dependent translational regulation. Cell Metab 18: 698-711

Nogueira V, Park Y, Chen CC, Xu PZ, Chen ML, Tonic I, Unterman T, Hay N (2008) Akt determines replicative senescence and oxidative or oncogenic premature senescence and sensitizes cells to oxidative apoptosis. Cancer Cell 14: 458-70

Patra KC, Hay N (2013) Hexokinase 2 as oncotarget. Oncotarget 4: 1862-3

Patra KC, Wang Q, Bhaskar PT, Miller L, Wang Z, Wheaton W, Chandel N, Laakso M, Muller WJ, Allen EL, Jha AK, Smolen GA, Clasquin MF, Robey RB, Hay N (2013) Hexokinase 2 is required for tumor initiation and maintenance and its systemic deletion is therapeutic in mouse models of cancer. Cancer Cell 24: 213-28

Piskounova E, Agathocleous M, Murphy MM, Hu Z, Huddlestun SE, Zhao Z, Leitch AM, Johnson TM, DeBerardinis RJ, Morrison SJ (2015) Oxidative stress inhibits distant metastasis by human melanoma cells. Nature 527: 186-91

Pourmand G, Ziaee AA, Abedi AR, Mehrsai A, Alavi HA, Ahmadi A, Saadati HR (2007) Role of PTEN gene in progression of prostate cancer. Urol J 4: 95-100

Rahman I, Kode A, Biswas SK (2006) Assay for quantitative determination of glutathione and glutathione disulfide levels using enzymatic recycling method. Nat Protoc 1: 3159-65

Roberts DJ, Tan-Sah VP, Ding EY, Smith JM, Miyamoto S (2014) Hexokinase-II positively regulates glucose starvation-induced autophagy through TORC1 inhibition. Mol Cell 53: 521-33

Robey RB, Hay N (2009) Is Akt the "Warburg kinase"?-Akt-energy metabolism interactions and oncogenesis. Semin Cancer Biol 19: 25-31

Sayin VI, Ibrahim MX, Larsson E, Nilsson JA, Lindahl P, Bergo MO (2014) Antioxidants accelerate lung cancer progression in mice. Science translational medicine 6: 221ra15

Skeen JE, Bhaskar PT, Chen CC, Chen WS, Peng XD, Nogueira V, Hahn-Windgassen A, Kiyokawa H, Hay N (2006) Akt deficiency impairs normal cell proliferation and suppresses oncogenesis in a p53-independent and mTORC1-dependent manner. Cancer Cell 10: 269-80

Taylor BS, Schultz N, Hieronymus H, Gopalan A, Xiao Y, Carver BS, Arora VK, Kaushik P, Cerami E, Reva B, Antipin Y, Mitsiades N, Landers T, Dolgalev I, Major JE, Wilson M, Socci ND, Lash AE, Heguy A, Eastham JA et al. (2010) Integrative genomic profiling of human prostate cancer. Cancer Cell 18: 11-22

Ting CM, Lee YM, Wong CK, Wong AS, Lung HL, Lung ML, Lo KW, Wong RN, Mak NK (2010) 2-Methoxyestradiol induces endoreduplication through the induction of mitochondrial oxidative stress and the activation of MAPK signaling pathways. Biochem Pharmacol 79: 825-41

Trotman LC, Niki M, Dotan ZA, Koutcher JA, Di Cristofano A, Xiao A, Khoo AS, Roy-Burman P, Greenberg NM, Van Dyke T, Cordon-Cardo C, Pandolfi PP (2003) Pten dose dictates cancer progression in the prostate. PLoS Biol 1: E59

Wang Q, Chen X, Hay N (2017) Akt as a target for cancer therapy: more is not always better (lessons from studies in mice). Br J Cancer 117: 159-163

Wang Q, Yu WN, Chen X, Peng XD, Jeon SM, Birnbaum MJ, Guzman G, Hay N (2016) Spontaneous Hepatocellular Carcinoma after the Combined Deletion of Akt Isoforms. Cancer Cell 29: 523-35

Xu K, Thornalley PJ (2001) Involvement of glutathione metabolism in the cytotoxicity of the phenethyl isothiocyanate and its cysteine conjugate to human leukaemia cells in vitro. Biochem Pharmacol 61: 165-77

Yu R, Mandlekar S, Harvey KJ, Ucker DS, Kong AN (1998) Chemopreventive isothiocyanates induce apoptosis and caspase-3-like protease activity. Cancer Res 58: 402-8

Zhang Y, Kwok-Shing Ng P, Kucherlapati M, Chen F, Liu Y, Tsang YH, de Velasco G, Jeong KJ, Akbani R, Hadjipanayis A, Pantazi A, Bristow CA, Lee E, Mahadeshwar HS, Tang J, Zhang J, Yang L, Seth S, Lee S, Ren X et al. (2017) A Pan-Cancer Proteogenomic Atlas of PI3K/AKT/mTOR Pathway Alterations. Cancer Cell 31: 820-832 e3

Zheng HC (2017) The molecular mechanisms of chemoresistance in cancers. Oncotarget 8: 59950-59964

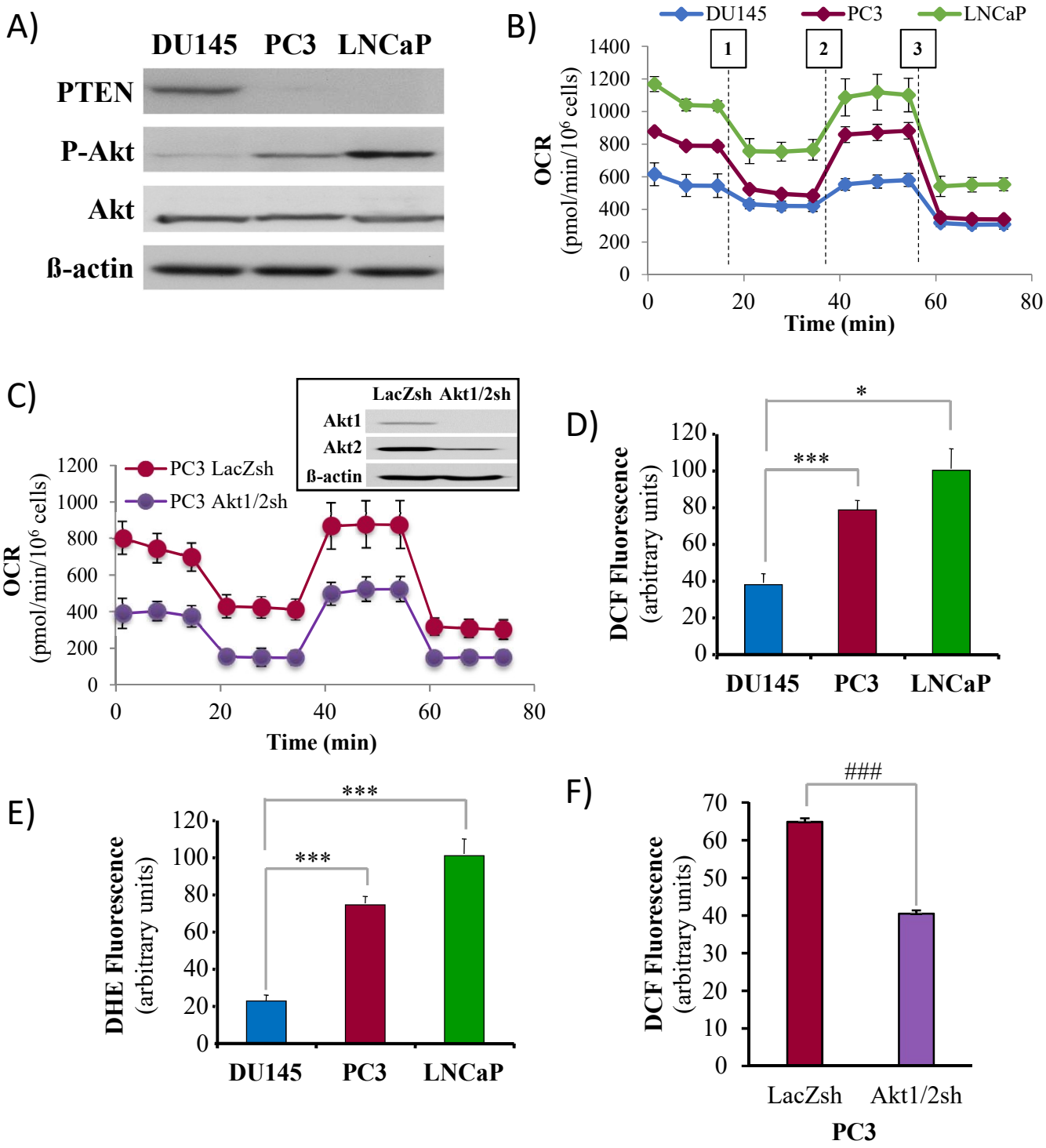
A)
DU145
PC3
LNCaP
PTEN
P-Akt
Akt
ß-actin
B)
DU145
PC3
LNCaP
1
2
3
OCR
(pmol/min/10⁶ cells)
Time (min)
C)
LacZsh
Akt1/2sh
Akt1
Akt2
ß-actin
PC3 LacZsh
PC3 Akt1/2sh
OCR
(pmol/min/10⁶ cells)
Time (min)
D)
DCF Fluorescence
(arbitrary units)
DU145
PC3
LNCaP
E)
DHE Fluorescence
(arbitrary units)
DU145
PC3
LNCaP
F)
DCF Fluorescence
(arbitrary units)
LacZsh
Akt1/2sh
PC3

Fig 1

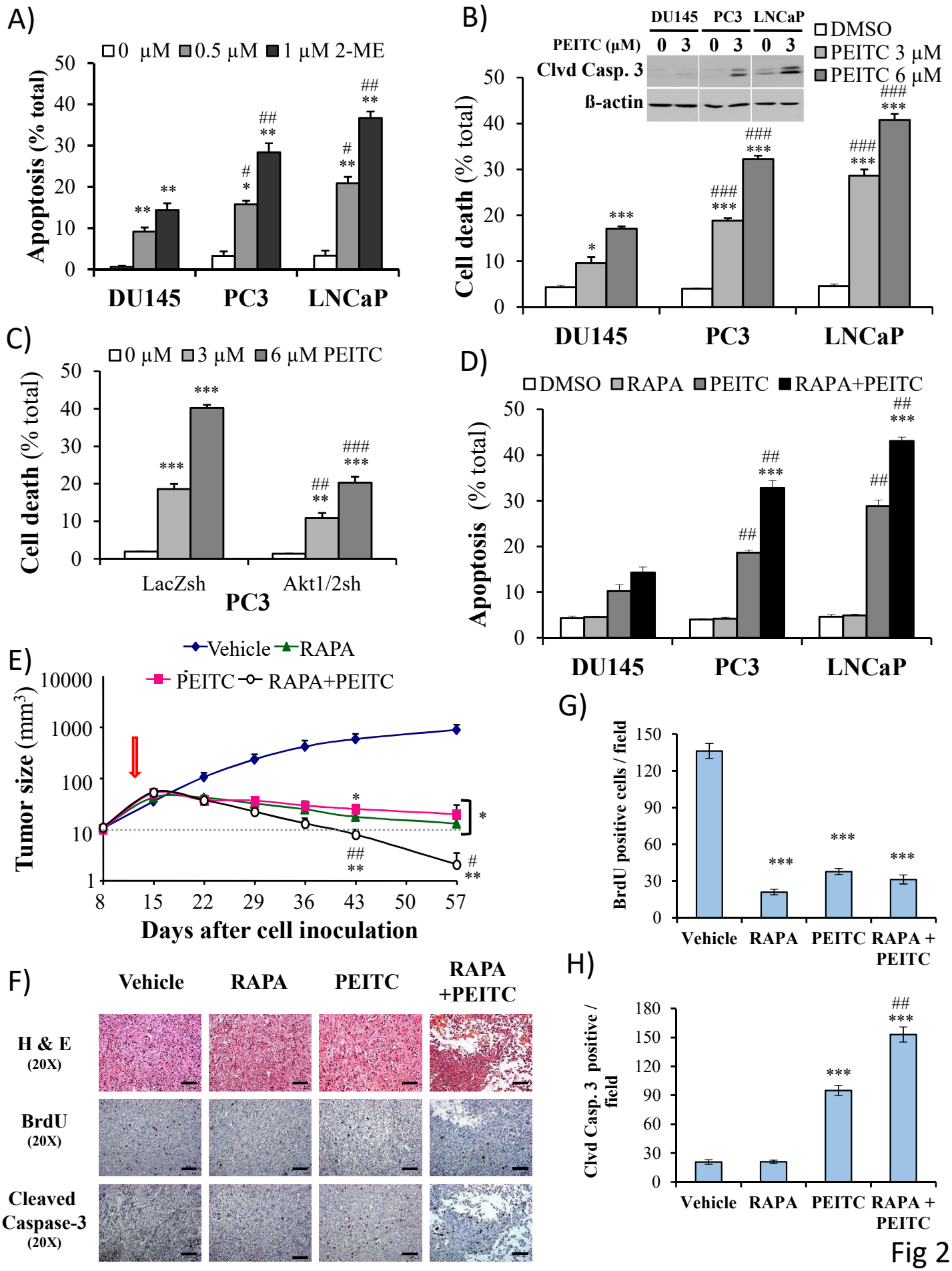
A)
0 μM 0.5 μM 1 μM 2-ME
Apoptosis (% total)
DU145
PC3
LNCaP
B)
DU145 PC3 LNCaP
PEITC (μM) 0 3 0 3 0 3
Clvd Casp. 3
ß-actin
DMSO
PEITC 3 μM
PEITC 6 μM
Cell death (% total)
DU145
PC3
LNCaP
C)
0 μM 3 μM 6 μM PEITC
Cell death (% total)
LacZsh
Akt1/2sh
PC3
D)
DMSO RAPA PEITC RAPA+PEITC
Apoptosis (% total)
DU145
PC3
LNCaP
E)
Vehicle RAPA
PEITC RAPA+PEITC
Tumor size (mm3)
Days after cell inoculation
G)
BrdU positive cells / field
Vehicle
RAPA
PEITC
RAPA + PEITC
F)
Vehicle
RAPA
PEITC
RAPA +PEITC
H & E (20X)
BrdU (20X)
Cleaved Caspase-3 (20X)
H)
Clvd Casp. 3 positive / field
Vehicle
RAPA
PEITC
RAPA + PEITC

Fig 2

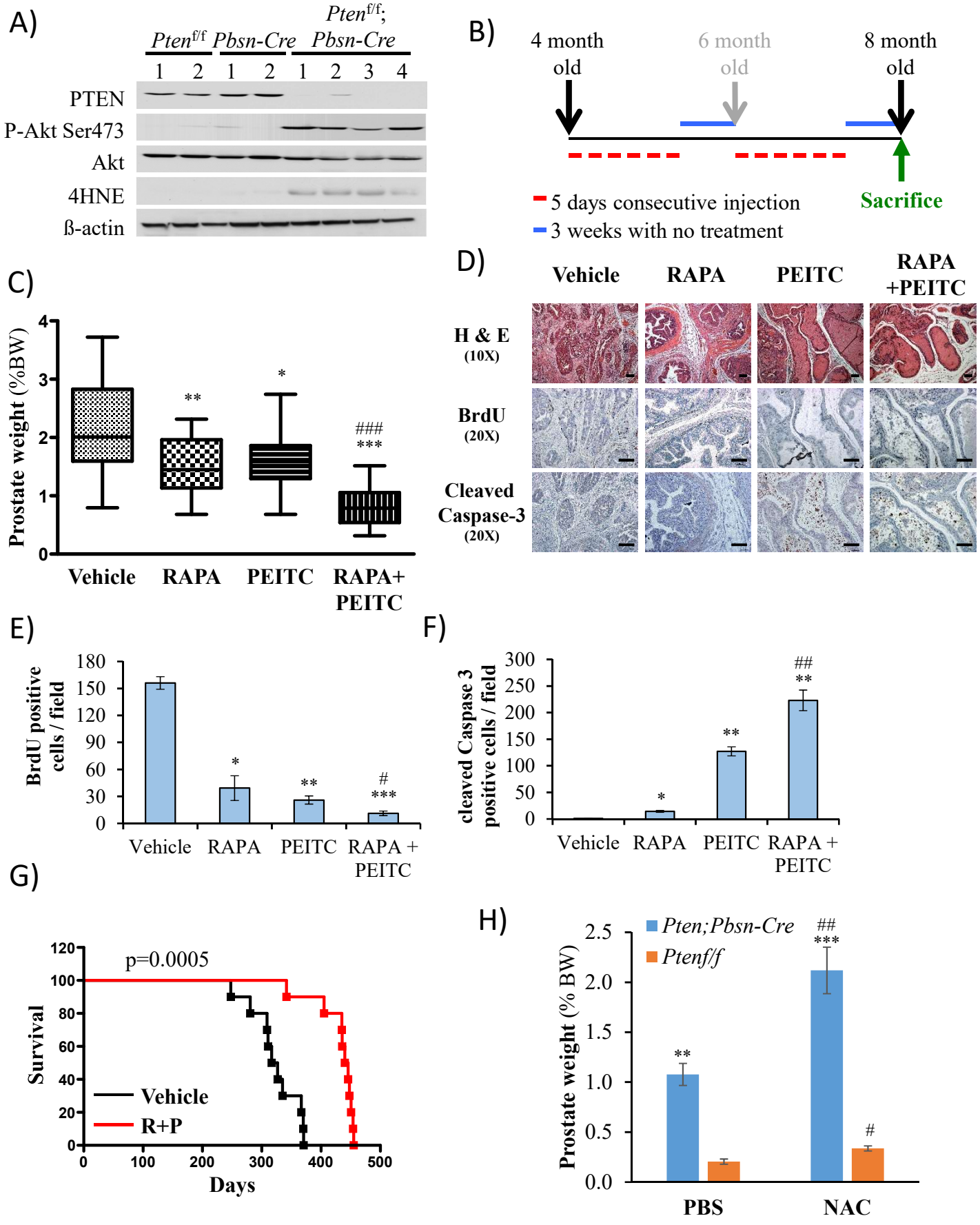
A)
Ptenf/f
Pbsn-Cre
Ptenf/f; Pbsn-Cre
1 2 1 2 1 2 3 4
PTEN
P-Akt Ser473
Akt
4HNE
ß-actin
B)
4 month old
6 month old
8 month old
5 days consecutive injection
3 weeks with no treatment
Sacrifice
C)
Prostate weight (%BW)
Vehicle
RAPA
PEITC
RAPA+ PEITC
D)
Vehicle
RAPA
PEITC
RAPA +PEITC
H & E (10X)
BrdU (20X)
Cleaved Caspase-3 (20X)
E)
BrdU positive cells / field
Vehicle
RAPA
PEITC
RAPA + PEITC
F)
cleaved Caspase 3 positive cells / field
Vehicle
RAPA
PEITC
RAPA + PEITC
G)
p=0.0005
Survival
Vehicle
R+P
Days
H)
Pten;Pbsn-Cre
Ptenf/f
Prostate weight (% BW)
PBS
NAC

Fig 3

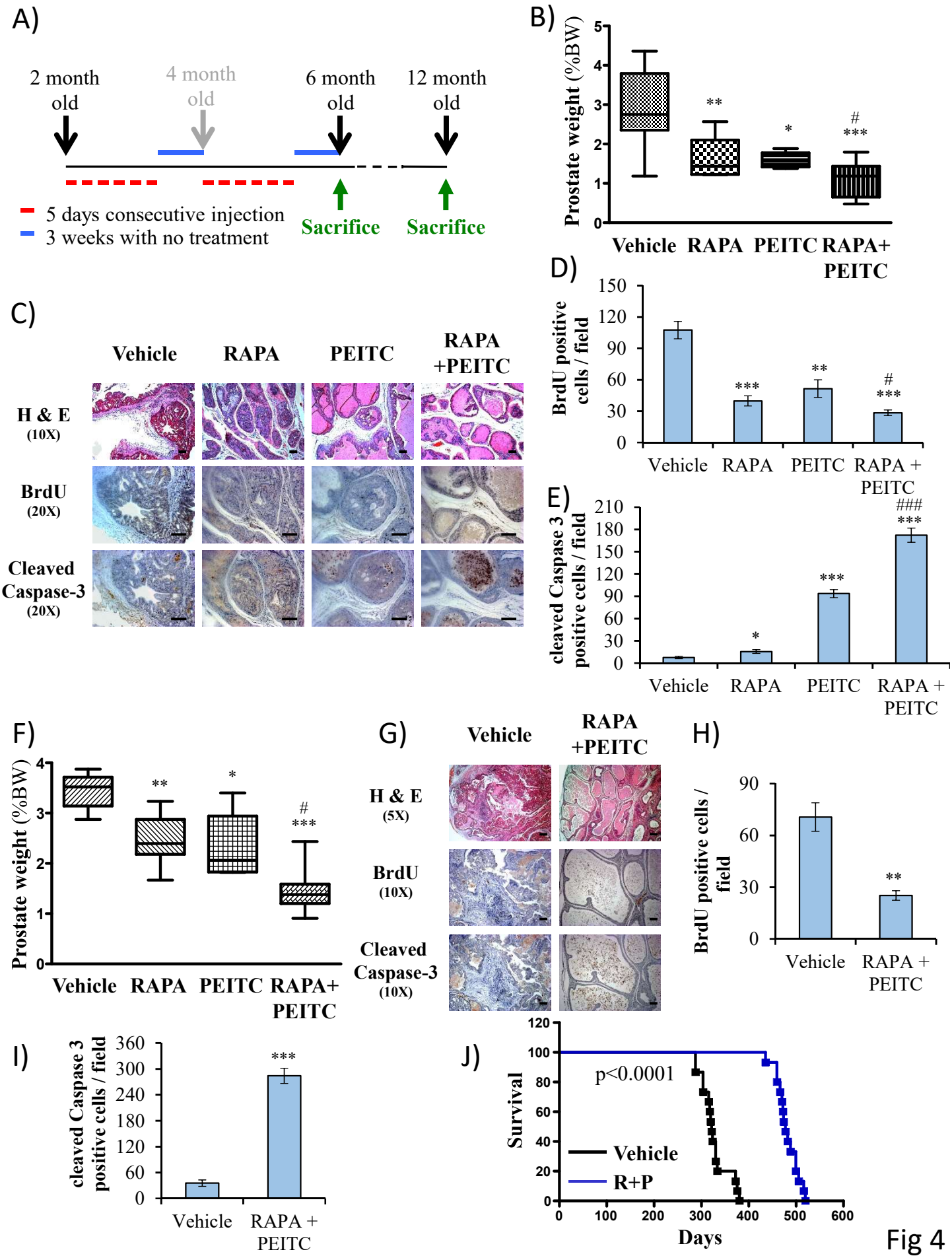
A)
2 month old
4 month old
6 month old
12 month old
5 days consecutive injection
3 weeks with no treatment
Sacrifice
Sacrifice
B)
Prostate weight (%BW)
Vehicle
RAPA
PEITC
RAPA+ PEITC
C)
Vehicle
RAPA
PEITC
RAPA +PEITC
H & E (10X)
BrdU (20X)
Cleaved Caspase-3 (20X)
D)
BrdU positive cells / field
Vehicle
RAPA
PEITC
RAPA + PEITC
E)
cleaved Caspase 3 positive cells / field
Vehicle
RAPA
PEITC
RAPA + PEITC
F)
Prostate weight (%BW)
Vehicle
RAPA
PEITC
RAPA+ PEITC
G)
Vehicle
RAPA +PEITC
H & E (5X)
BrdU (10X)
Cleaved Caspase-3 (10X)
H)
BrdU positive cells / field
Vehicle
RAPA + PEITC
I)
cleaved Caspase 3 positive cells / field
Vehicle
RAPA + PEITC
J)
Survival
p<0.0001
Vehicle
R+P
Days

Fig 4

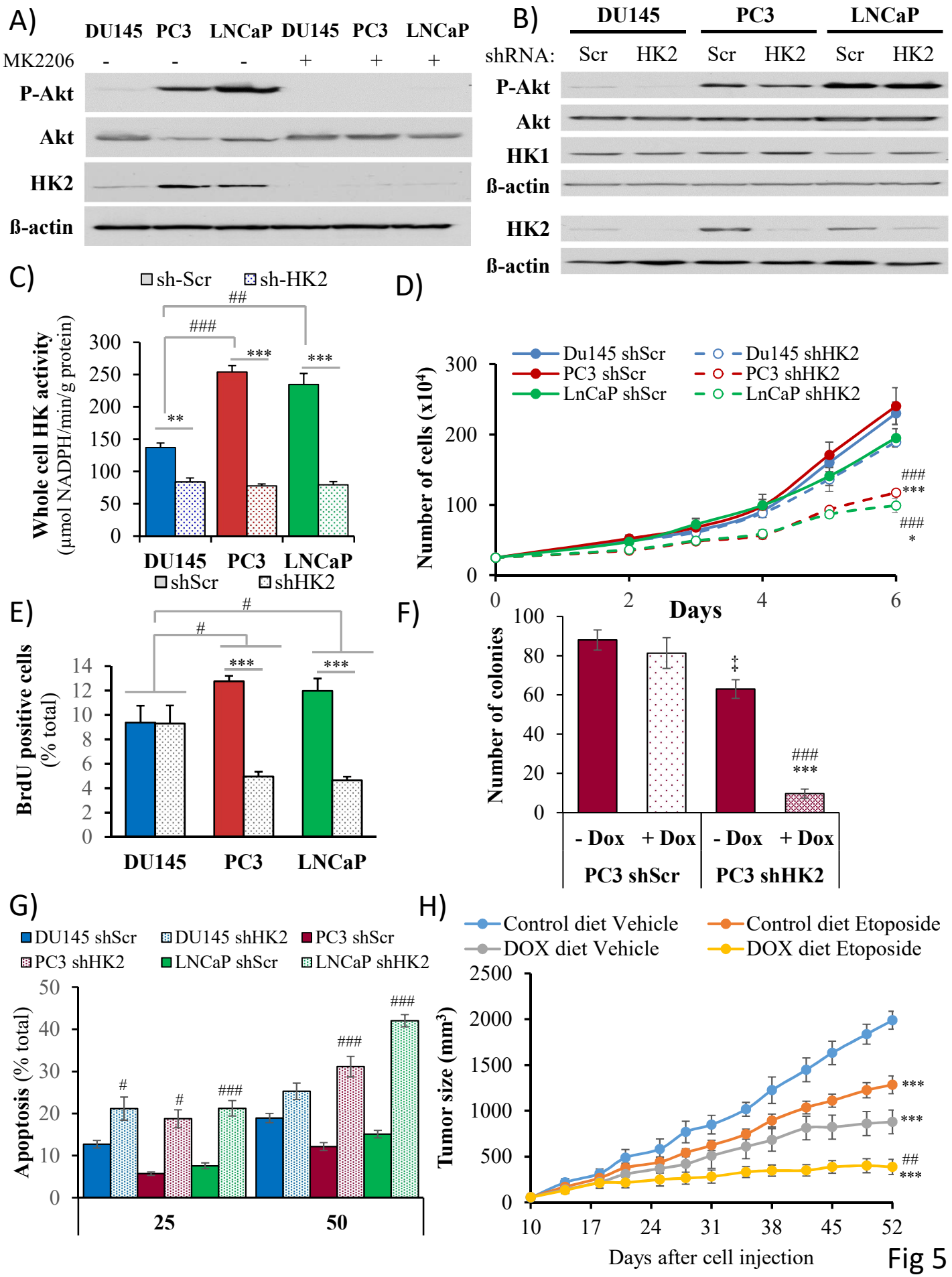
A)
DU145 PC3 LNCaP DU145 PC3 LNCaP
MK2206 - - - + + +
P-Akt
Akt
HK2
ß-actin
B)
DU145 PC3 LNCaP
shRNA: Scr HK2 Scr HK2 Scr HK2
P-Akt
Akt
HK1
ß-actin
HK2
ß-actin
C)
sh-Scr sh-HK2
Whole cell HK activity (µmol NADPH/min/g protein)
DU145 PC3 LNCaP
shScr shHK2
D)
Du145 shScr
PC3 shScr
LnCaP shScr
Du145 shHK2
PC3 shHK2
LnCaP shHK2
Number of cells (x10⁴)
Days
E)
BrdU positive cells (% total)
DU145 PC3 LNCaP
F)
Number of colonies
- Dox + Dox - Dox + Dox
PC3 shScr PC3 shHK2
G)
DU145 shScr
DU145 shHK2
PC3 shScr
PC3 shHK2
LNCaP shScr
LNCaP shHK2
Apoptosis (% total)
25 50
H)
Control diet Vehicle
Control diet Etoposide
DOX diet Vehicle
DOX diet Etoposide
Tumor size (mm³)
Days after cell injection

Fig 5

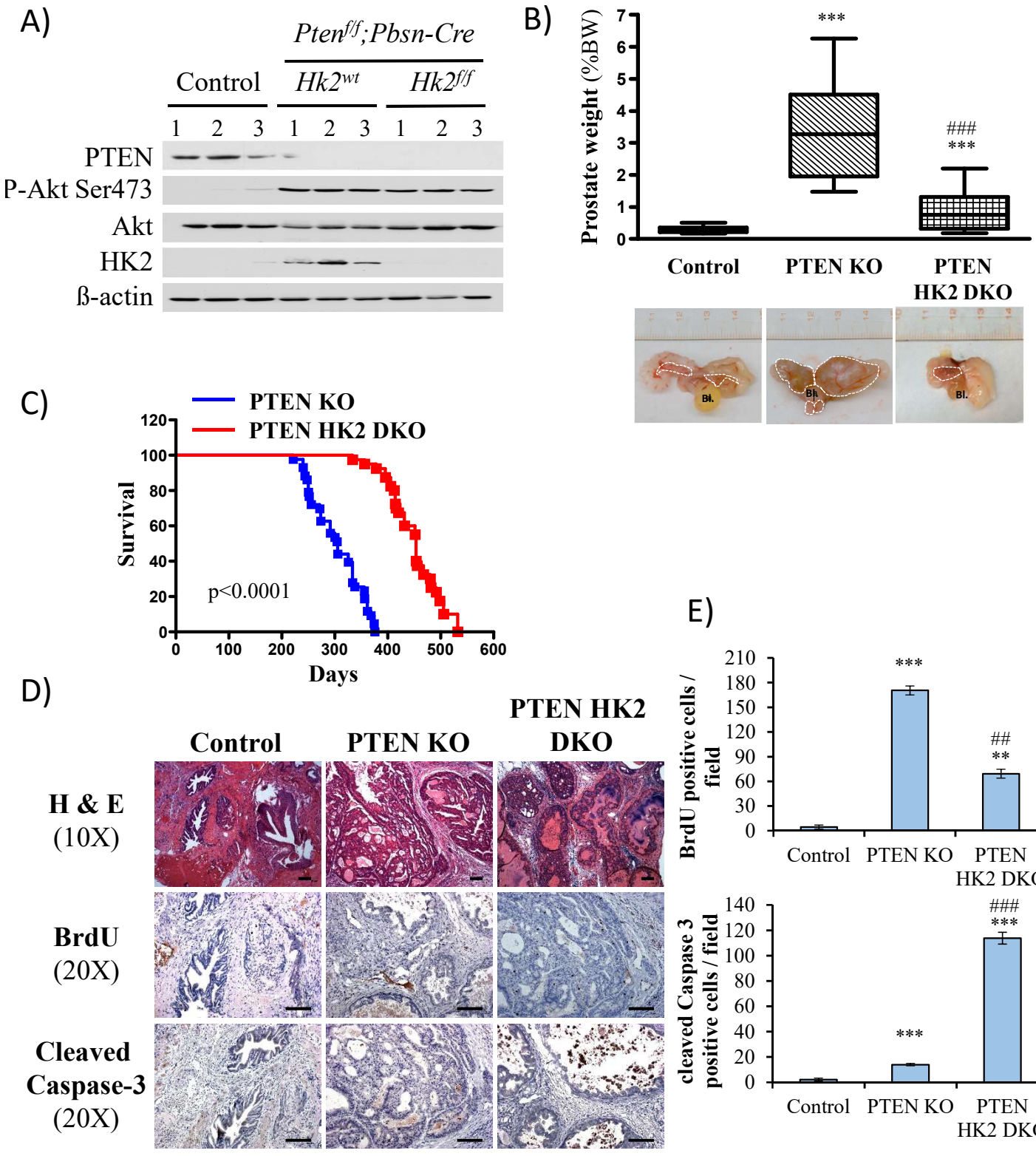
A)
Pten f/f;Pbsn-Cre
Control
Hk2 wt
Hk2 f/f
1 2 3 1 2 3 1 2 3
PTEN
P-Akt Ser473
Akt
HK2
ß-actin
B)
Prostate weight (%BW)
***
###
***
Control
PTEN KO
PTEN HK2 DKO
Bl.
C)
PTEN KO
PTEN HK2 DKO
Survival
p<0.0001
Days
D)
Control
PTEN KO
PTEN HK2 DKO
H & E (10X)
BrdU (20X)
Cleaved Caspase-3 (20X)
E)
BrdU positive cells / field
***
##
**
Control
PTEN KO
PTEN HK2 DKO
cleaved Caspase 3 positive cells / field
***
###
***
Control
PTEN KO
PTEN HK2 DKO

Fig 6

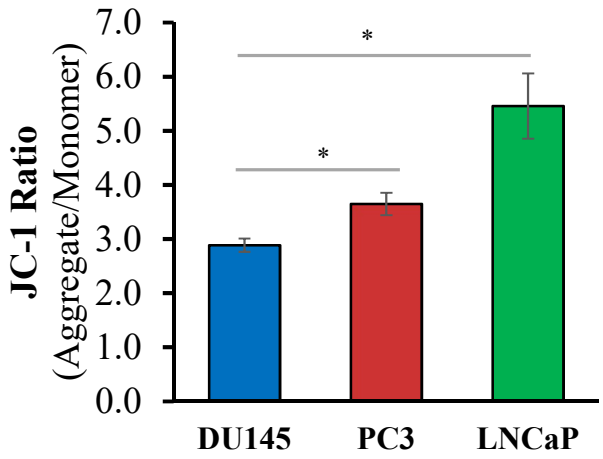
JC-1 Ratio
(Aggregate/Monomer)
7.0
6.0
5.0
4.0
3.0
2.0
1.0
0.0
*
*
DU145
PC3
LNCaP

Figure 1s1

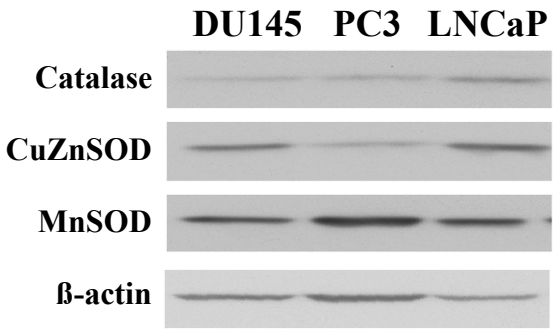

Figure 1s2

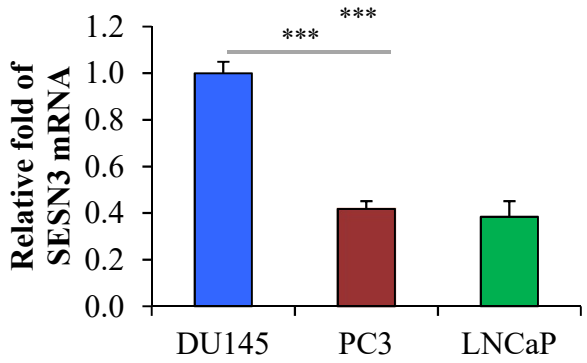
Relative fold of SESN3 mRNA
1.2
1.0
0.8
0.6
0.4
0.2
0.0
***
***
DU145
PC3
LNCaP

Figure 1s3

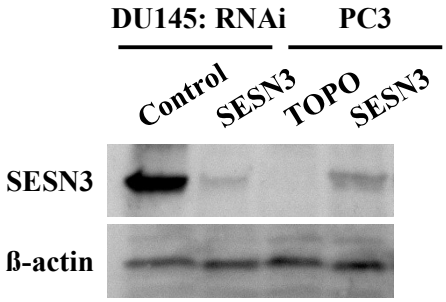

Figure 1s4

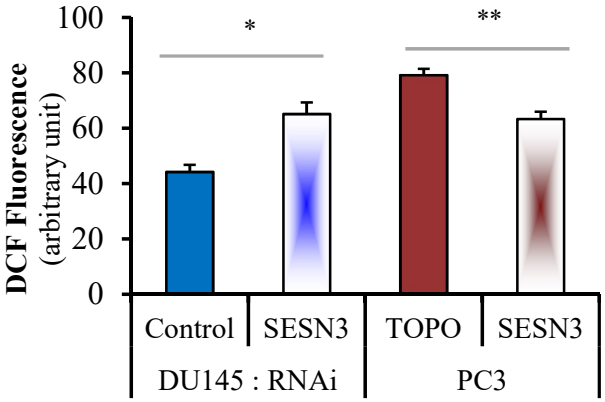
100
80
60
40
20
0
DCF Fluorescence
(arbitrary unit)
*
**
Control
SESN3
TOPO
SESN3
DU145 : RNAi
PC3

Figure 1s5

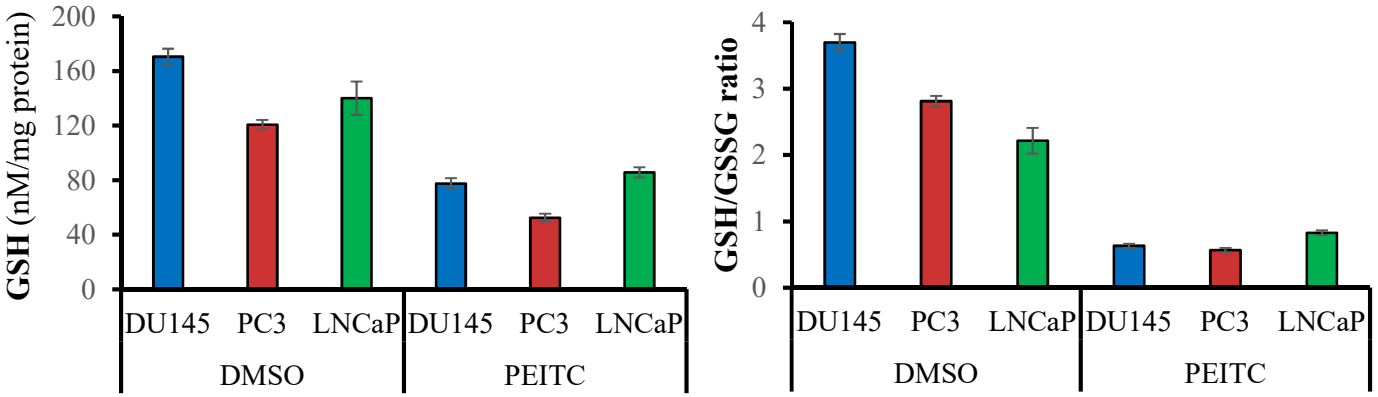
GSH (nM/mg protein)
200
160
120
80
40
0
DU145
PC3
LNCaP
DU145
PC3
LNCaP
DMSO
PEITC
GSH/GSSG ratio
4
3
2
1
0
DU145
PC3
LNCaP
DU145
PC3
LNCaP
DMSO
PEITC

Figure 2s1

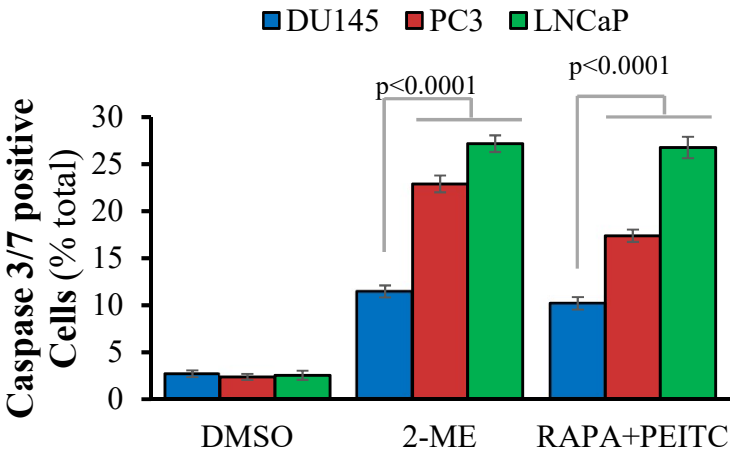
DU145
PC3
LNCaP
Caspase 3/7 positive Cells (% total)
30
25
20
15
10
5
0
p<0.0001
p<0.0001
DMSO
2-ME
RAPA+PEITC

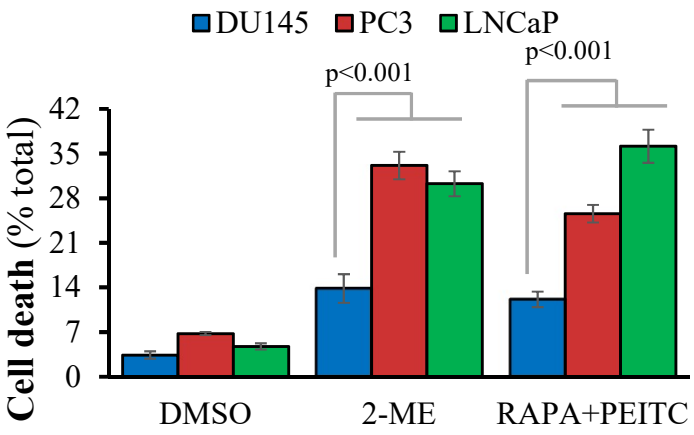
DU145
PC3
LNCaP
Cell death (% total)
42
35
28
21
14
7
0
p<0.001
p<0.001
DMSO
2-ME
RAPA+PEITC

Figure 2s2

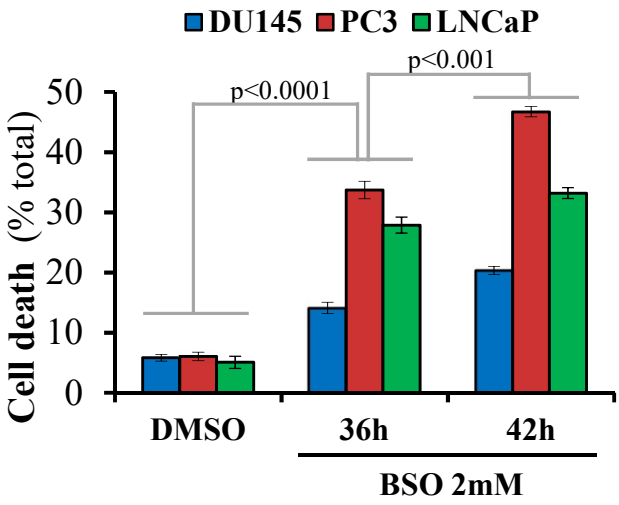
DU145
PC3
LNCaP
p<0.001
p<0.0001
Cell death (% total)
50
40
30
20
10
0
DMSO
36h
42h
BSO 2mM

Figure 2s3

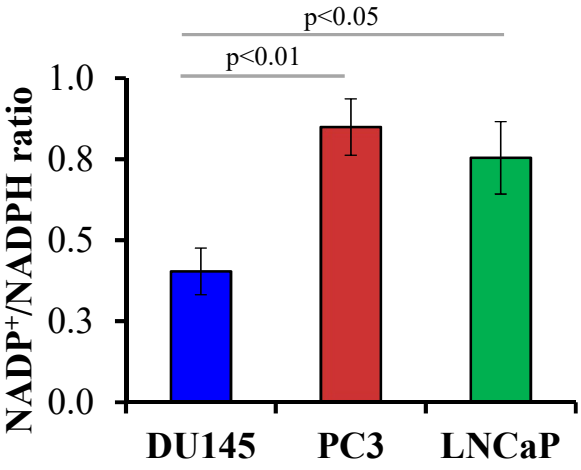

Figure 2s4

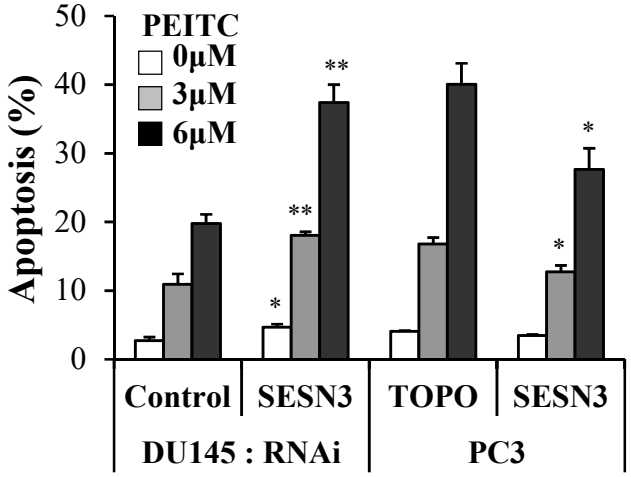
PEITC
0μM
3μM
6μM
Apoptosis (%)
50
40
30
20
10
0
*
**
**
*
*
Control
SESN3
TOPO
SESN3
DU145 : RNAi
PC3

Figure 2s5

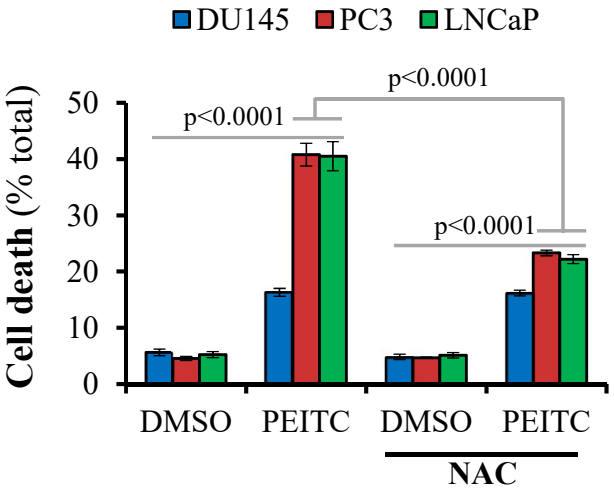
DU145
PC3
LNCaP
Cell death (% total)
50
40
30
20
10
0
p<0.0001
p<0.0001
p<0.0001
DMSO
PEITC
DMSO
PEITC
NAC

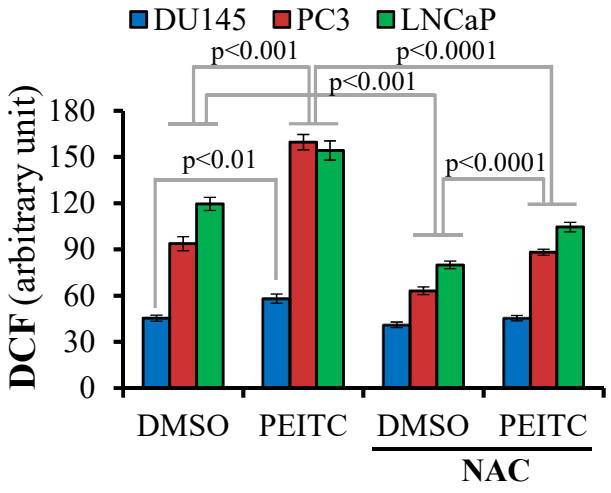
DU145
PC3
LNCaP
DCF (arbitrary unit)
180
150
120
90
60
30
0
p<0.001
p<0.0001
p<0.001
p<0.01
p<0.0001
DMSO
PEITC
DMSO
PEITC
NAC

Figure 2s6

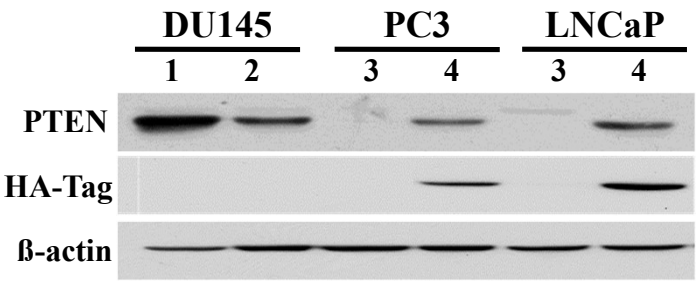

1: shLacZ 3: pBP
2: shPTEN 4: pBP-PTEN-HA

Figure 2s7

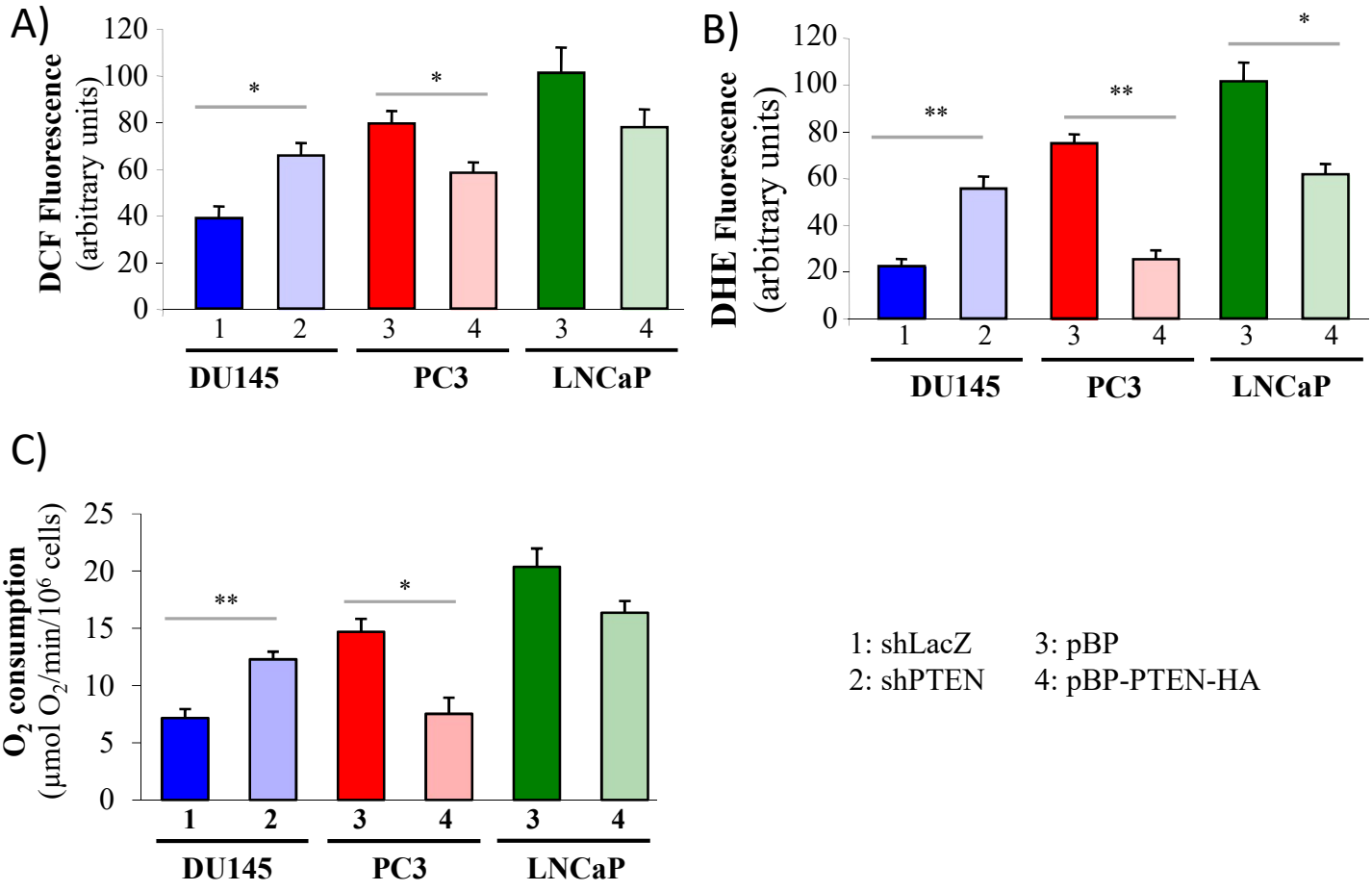
A)
DCF Fluorescence
(arbitrary units)
120
100
80
60
40
20
0
*
*
1
2
3
4
3
4
DU145
PC3
LNCaP
B)
DHE Fluorescence
(arbitrary units)
120
100
80
60
40
20
0
**
**
*
1
2
3
4
3
4
DU145
PC3
LNCaP
C)
O2 consumption
(µmol O2/min/10^6 cells)
25
20
15
10
5
0
**
*
1
2
3
4
3
4
DU145
PC3
LNCaP
1: shLacZ
2: shPTEN
3: pBP
4: pBP-PTEN-HA

Figure 2s8

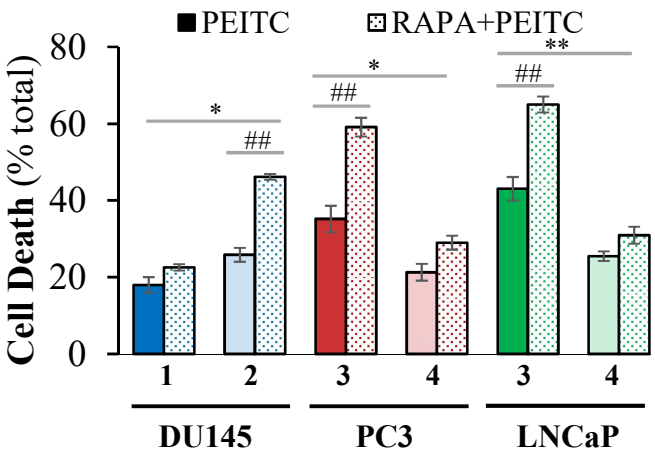

1: shLacZ 3: pBP
2: shPTEN 4: pBP-PTEN-HA

Figure 2s9

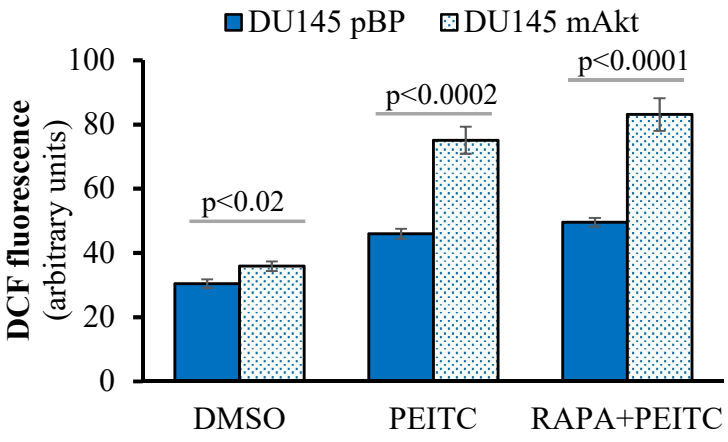
DU145 pBP
DU145 mAkt
DCF fluorescence
(arbitrary units)
100
80
60
40
20
0
p<0.02
p<0.0002
p<0.0001
DMSO
PEITC
RAPA+PEITC

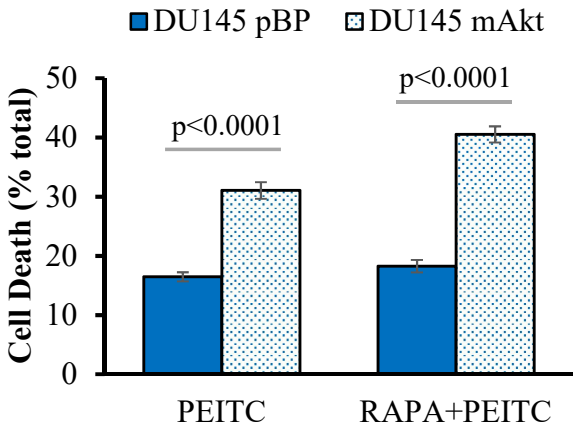
DU145 pBP
DU145 mAkt
Cell Death (% total)
50
40
30
20
10
0
p<0.0001
p<0.0001
PEITC
RAPA+PEITC

Figure 2s10

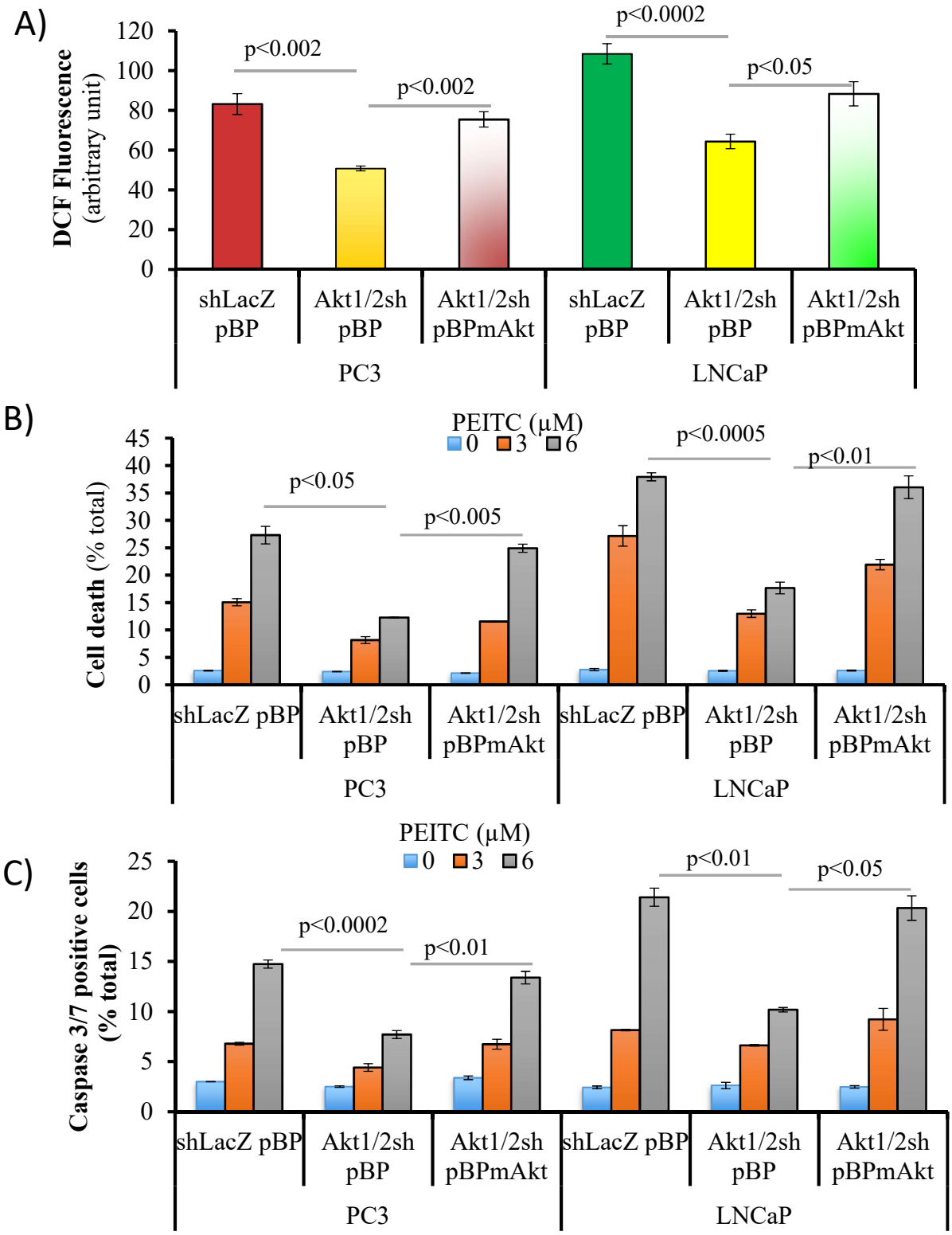
A)
DCF Fluorescence (arbitrary unit)
120
100
80
60
40
20
0
p<0.002
p<0.002
p<0.0002
p<0.05
shLacZ pBP
Akt1/2sh pBP
Akt1/2sh pBPmAkt
shLacZ pBP
Akt1/2sh pBP
Akt1/2sh pBPmAkt
PC3
LNCaP
B)
PEITC (μM)
0 3 6
Cell death (% total)
45
40
35
30
25
20
15
10
5
0
p<0.05
p<0.005
p<0.0005
p<0.01
shLacZ pBP
Akt1/2sh pBP
Akt1/2sh pBPmAkt
shLacZ pBP
Akt1/2sh pBP
Akt1/2sh pBPmAkt
PC3
LNCaP
C)
PEITC (μM)
0 3 6
Caspase 3/7 positive cells (% total)
25
20
15
10
5
0
p<0.0002
p<0.01
p<0.01
p<0.05
shLacZ pBP
Akt1/2sh pBP
Akt1/2sh pBPmAkt
shLacZ pBP
Akt1/2sh pBP
Akt1/2sh pBPmAkt
PC3
LNCaP

Figure 2s11

A)

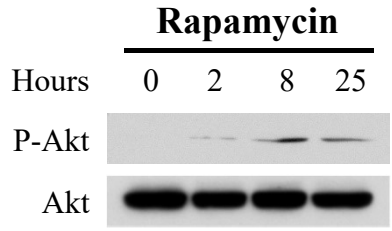

B)

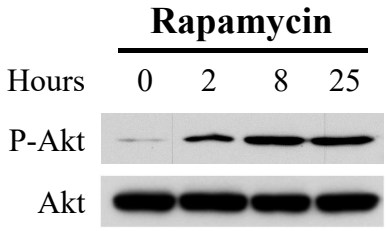

C)

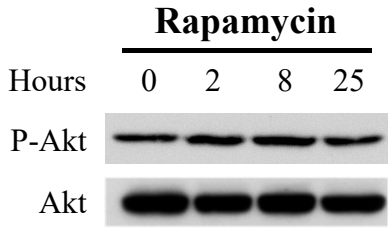

D)

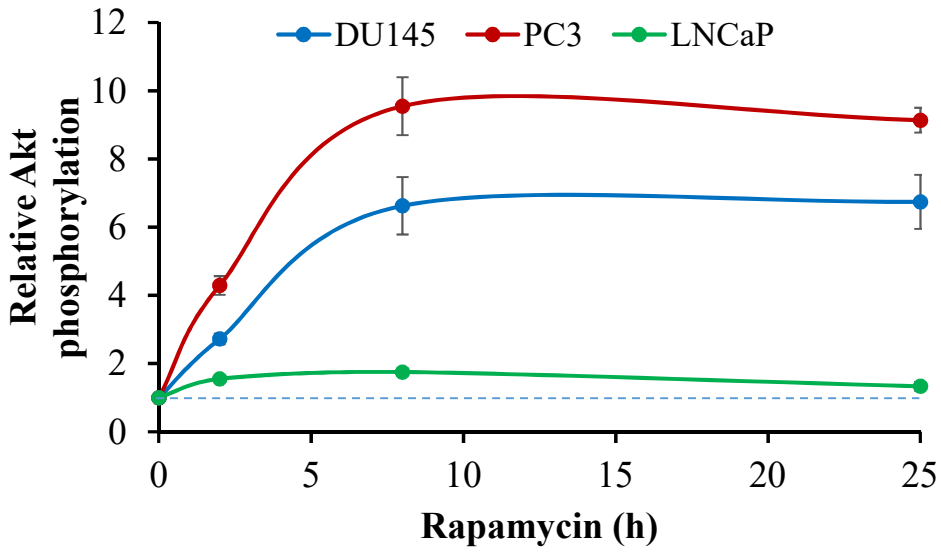

Figure 2s12

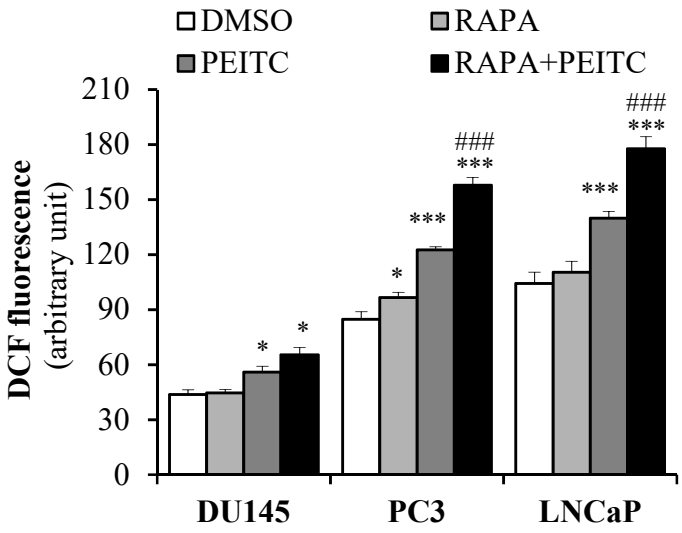
DMSO
RAPA
PEITC
RAPA+PEITC
DCF fluorescence
(arbitrary unit)
210
180
150
120
90
60
30
0
*
*
*
***
###
***
***
###
***
DU145
PC3
LNCaP

Figure 2s13

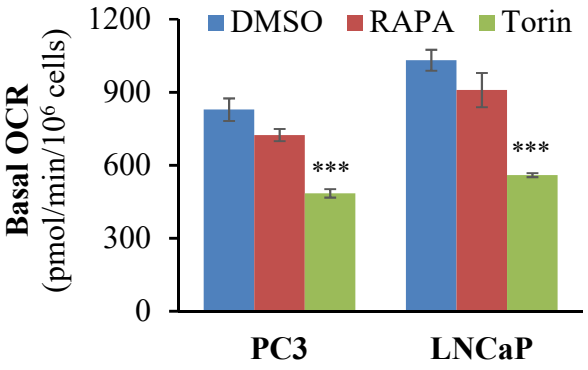
Basal OCR
(pmol/min/10^6 cells)
1200
900
600
300
0
DMSO
RAPA
Torin
***
***
PC3
LNCaP

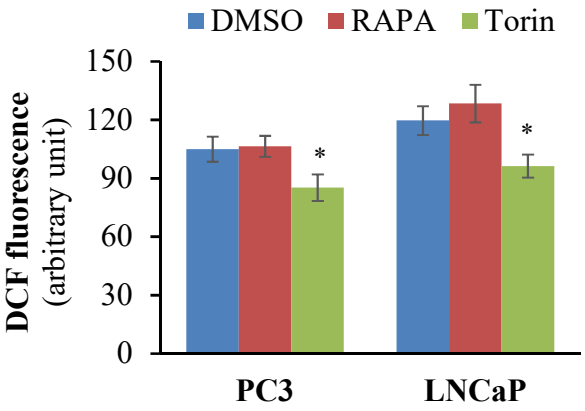
DCF fluorescence
(arbitrary unit)
150
120
90
60
30
0
DMSO
RAPA
Torin
*
*
PC3
LNCaP

Figure 2s14

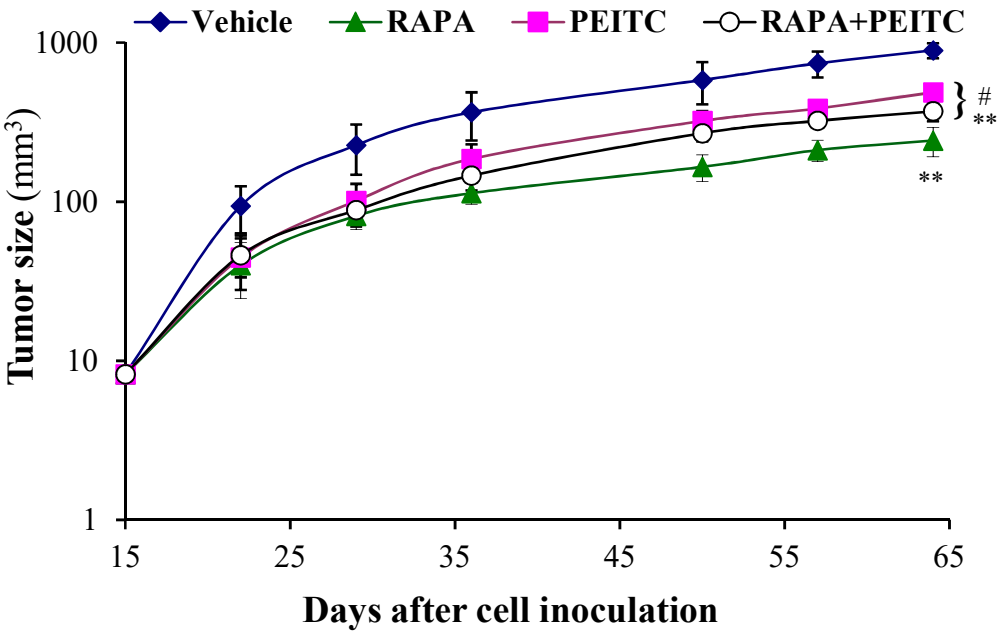
Vehicle
RAPA
PEITC
RAPA+PEITC
1000
100
10
1
Tumor size (mm3)
15
25
35
45
55
65
Days after cell inoculation
#
**
**

Figure 2s15

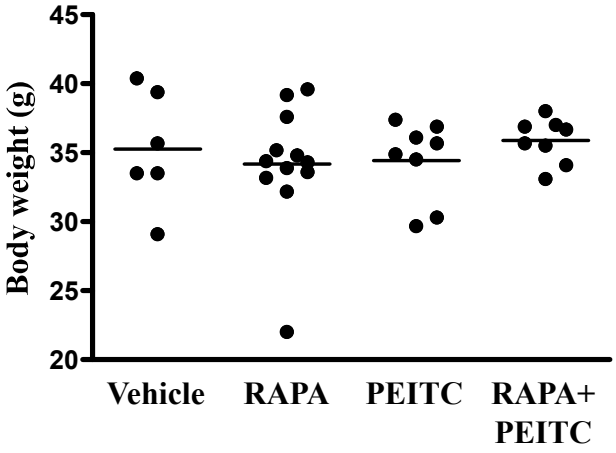
Body weight (g)
45
40
35
30
25
20
Vehicle
RAPA
PEITC
RAPA+
PEITC

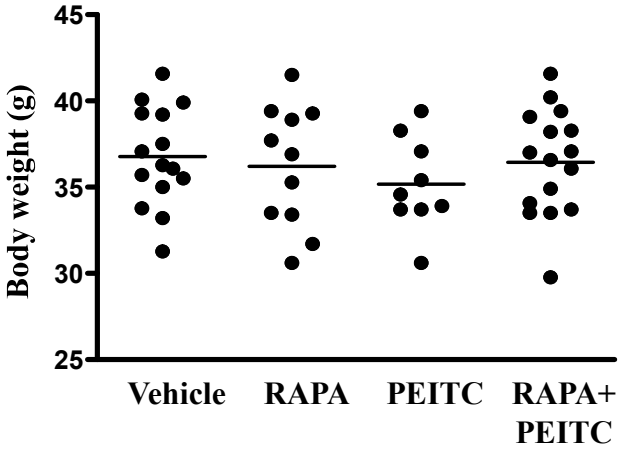
Body weight (g)
45
40
35
30
25
Vehicle
RAPA
PEITC
RAPA+
PEITC

Figure 3s1

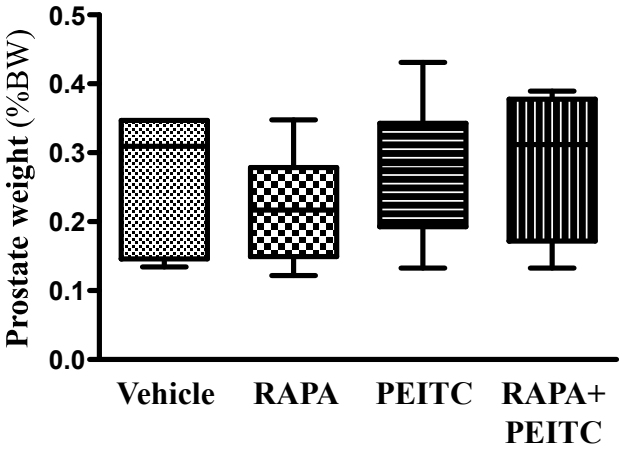
Prostate weight (%BW)
0.5
0.4
0.3
0.2
0.1
0.0
Vehicle
RAPA
PEITC
RAPA+
PEITC

Figure 3s2

	−	R+P	NAC
No PIN		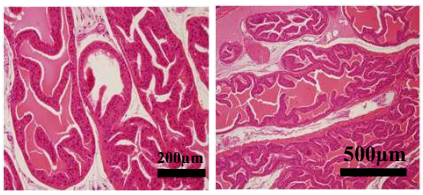	
Low Grade PIN		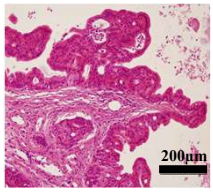	
High Grade PIN	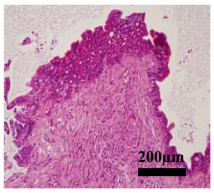 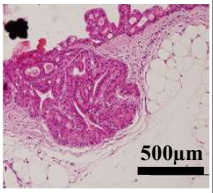	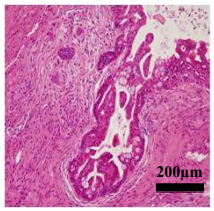	
Microinvasive Carcinoma	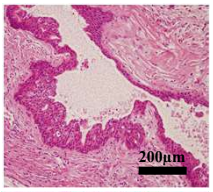 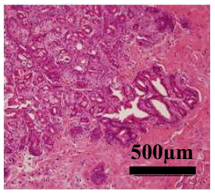	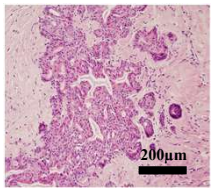	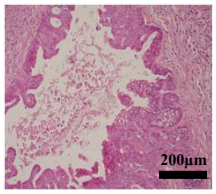
Invasive Carcinoma			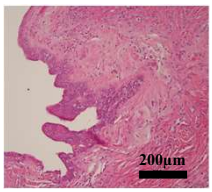 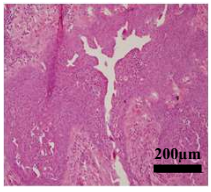 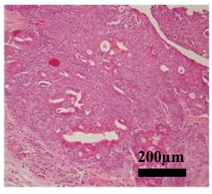

Figure 3s3

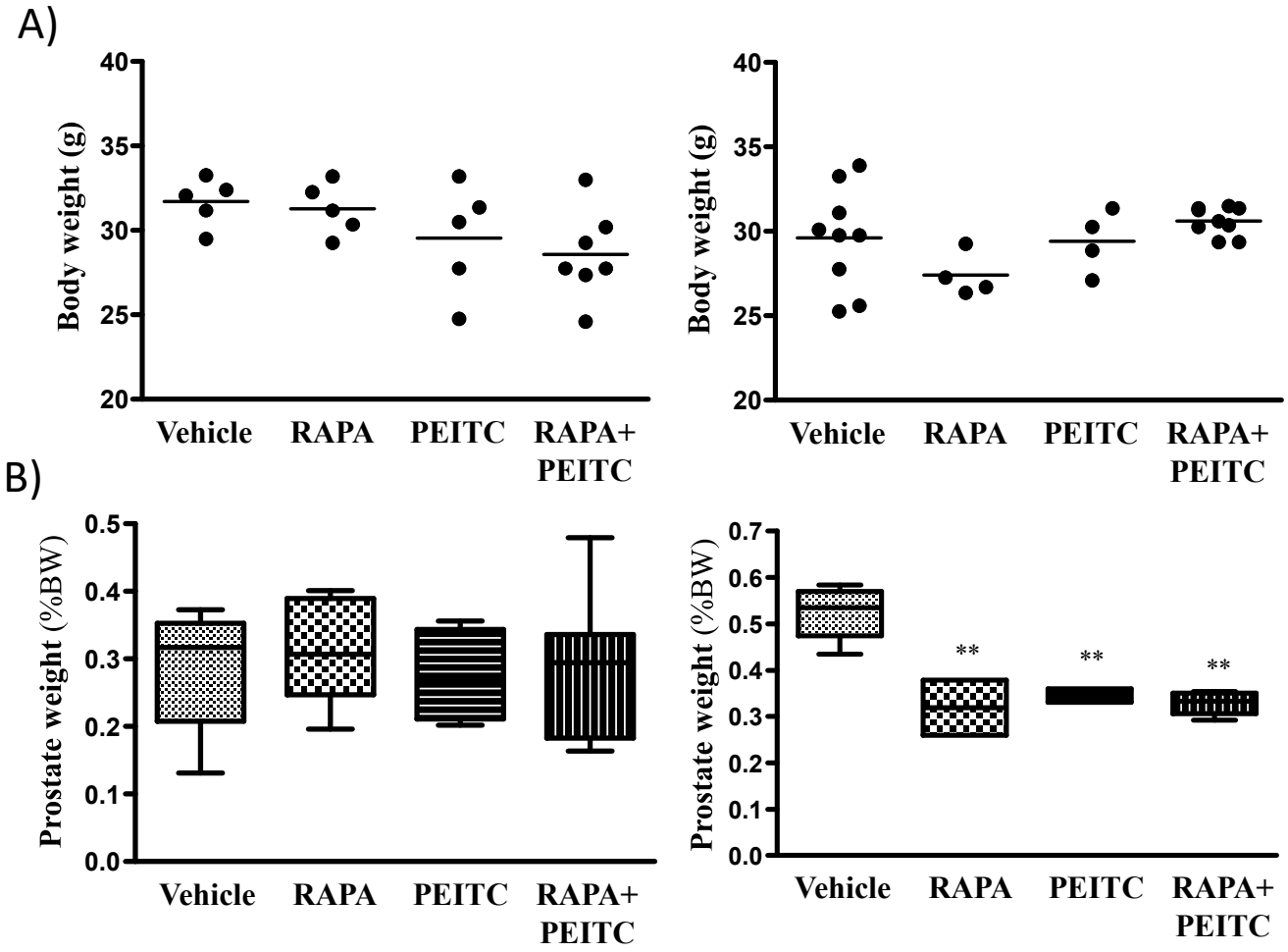
A)
Body weight (g)
40
35
30
25
20
Vehicle
RAPA
PEITC
RAPA+ PEITC
Body weight (g)
40
35
30
25
20
Vehicle
RAPA
PEITC
RAPA+ PEITC
B)
Prostate weight (%BW)
0.5
0.4
0.3
0.2
0.1
0.0
Vehicle
RAPA
PEITC
RAPA+ PEITC
Prostate weight (%BW)
0.7
0.6
0.5
0.4
0.3
0.2
0.1
0.0
**
**
**
Vehicle
RAPA
PEITC
RAPA+ PEITC

Figure 4s1

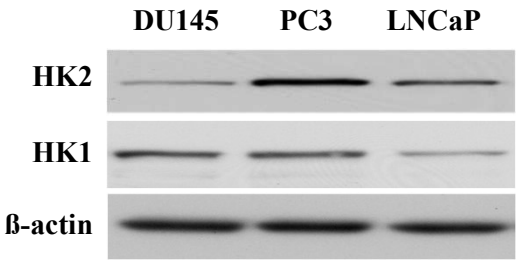

Figure 5s1

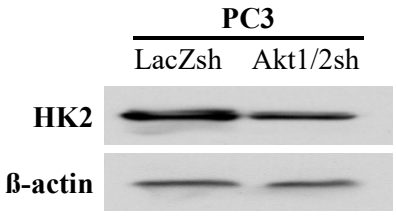

Figure 5s2

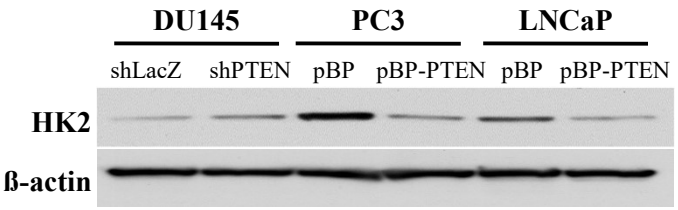
DU145
PC3
LNCaP
shLacZ
shPTEN
pBP
pBP-PTEN
pBP
pBP-PTEN
HK2
ß-actin

Figure 5s3

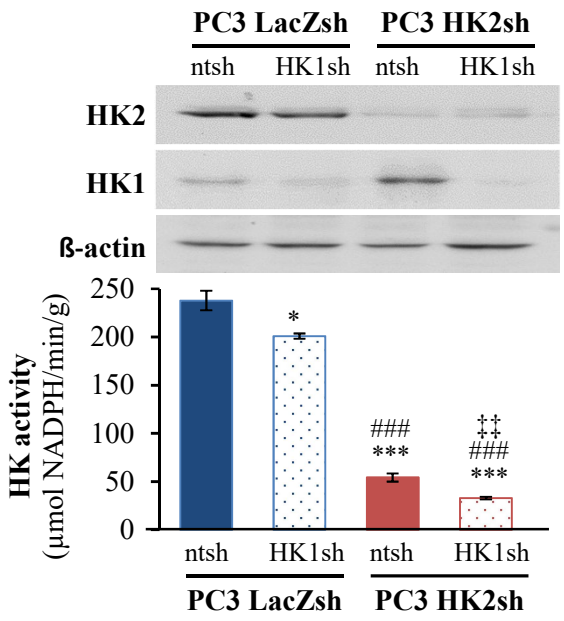
PC3 LacZsh
PC3 HK2sh
ntsh
HK1sh
ntsh
HK1sh
HK2
HK1
ß-actin
HK activity
(µmol NADPH/min/g)
250
200
150
100
50
0
*
###
***
‡‡
###
***
ntsh
HK1sh
ntsh
HK1sh
PC3 LacZsh
PC3 HK2sh

Figure 5s4

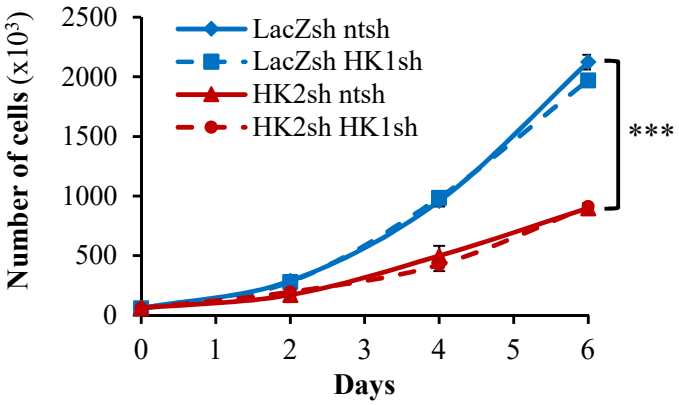
Number of cells (x10³)
2500
2000
1500
1000
500
0
0
1
2
3
4
5
6
Days
LacZsh ntsh
LacZsh HK1sh
HK2sh ntsh
HK2sh HK1sh
***

Figure 5s5

A)

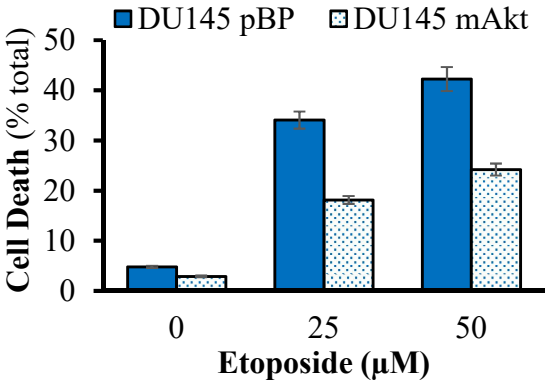

B)

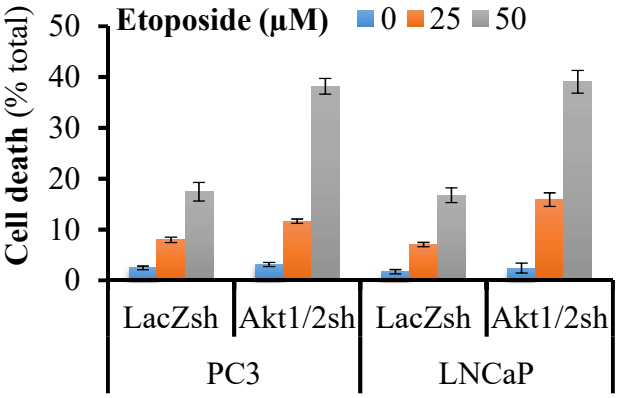

Figure 5s6

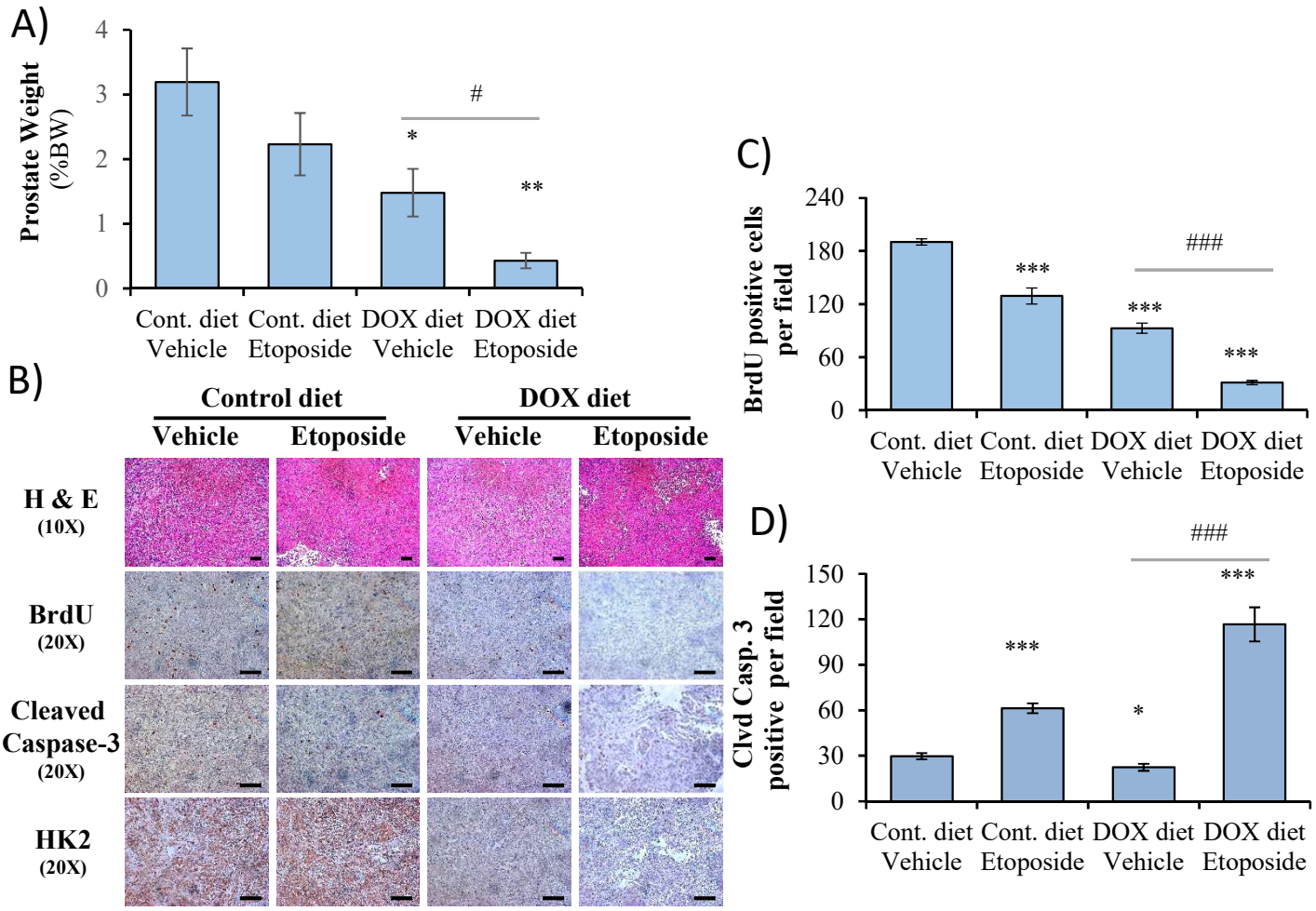
A)
Prostate Weight (%BW)
4
3
2
1
0
#
*
**
Cont. diet Vehicle
Cont. diet Etoposide
DOX diet Vehicle
DOX diet Etoposide
B)
Control diet
DOX diet
Vehicle
Etoposide
Vehicle
Etoposide
H & E (10X)
BrdU (20X)
Cleaved Caspase-3 (20X)
HK2 (20X)
C)
BrdU positive cells per field
240
180
120
60
0
###
***
***
***
Cont. diet Vehicle
Cont. diet Etoposide
DOX diet Vehicle
DOX diet Etoposide
D)
Clvd Casp. 3 positive per field
150
120
90
60
30
0
###
***
***
*
Cont. diet Vehicle
Cont. diet Etoposide
DOX diet Vehicle
DOX diet Etoposide

Figure 5s7

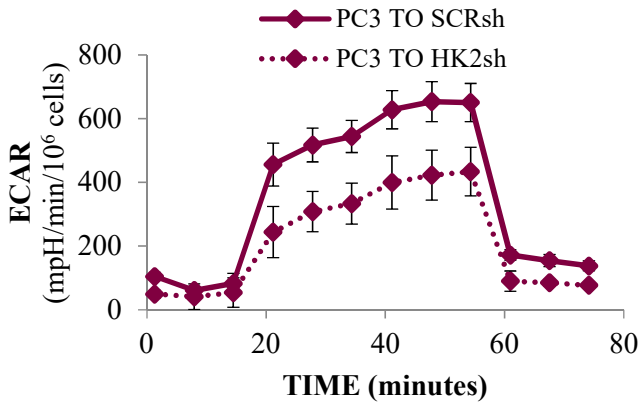
PC3 TO SCRsh
PC3 TO HK2sh
ECAR
(mpH/min/10^6 cells)
800
600
400
200
0
0
20
40
60
80
TIME (minutes)

Figure 5s8

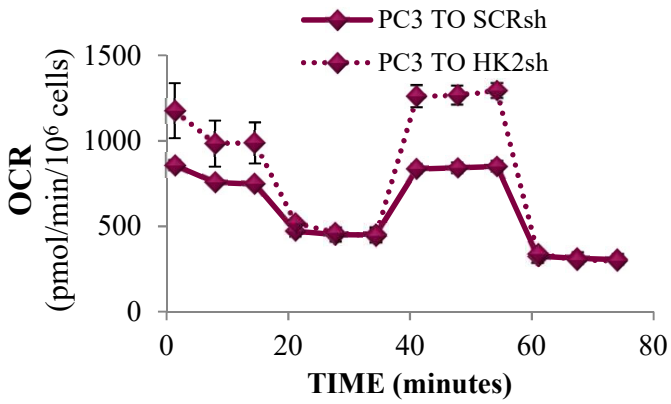
PC3 TO SCRsh
PC3 TO HK2sh
OCR
(pmol/min/10^6 cells)
1500
1000
500
0
0
20
40
60
80
TIME (minutes)

Figure 5s9

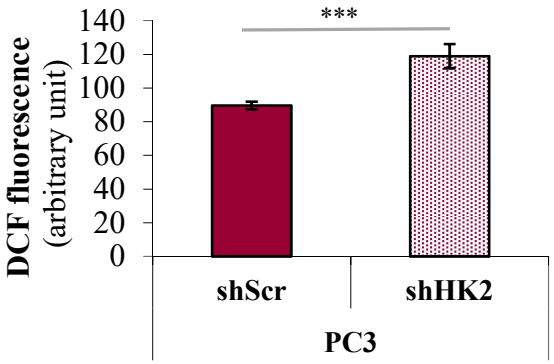
***
140
120
100
80
60
40
20
0
DCF fluorescence
(arbitrary unit)
shScr
shHK2
PC3

Figure 5s10

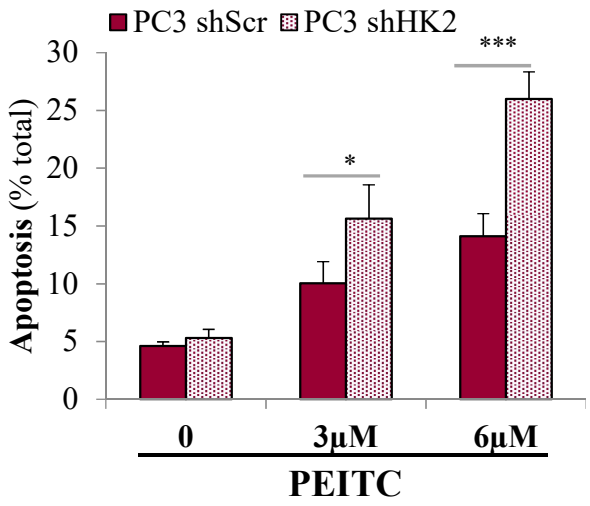
PC3 shScr
PC3 shHK2
Apoptosis (% total)
30
25
20
15
10
5
0
*
***
0
3µM
6µM
PEITC

Figure 5s11